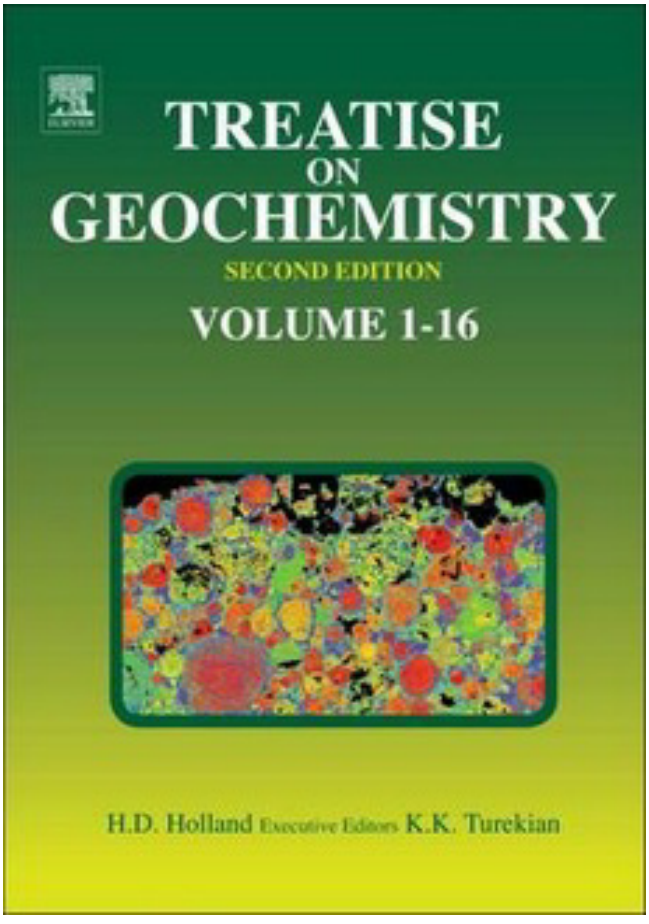

Bina C.R., and Helffrich G. (2014) Geophysical Constraints on Mantle Composition. In: Holland H.D. and Turekian K.K. (eds.) Treatise on Geochemistry, Second Edition, vol. 3, pp. 41-65. Oxford: Elsevier.

3.2 Geophysical Constraints on Mantle Composition

CR Bina, Northwestern University, Evanston, IL, USA
G Helffrich, University of Bristol, Bristol, UK

This article is a revision of the previous edition article by C R Bina, volume 2, pp. 39–59, © 2003, Elsevier Ltd.

3.2.1 Introduction

3.2.1.1 General Considerations

Direct sampling of mantle rocks and minerals is limited to tectonic slices emplaced at the surface (Chapter 3.4), smaller xenoliths transported upward by magmatic processes (Chapter 3.5), and still smaller inclusions in such far-traveled natural sample chambers as diamonds (Chapter 3.5). Because of such limited direct access to mantle materials, knowledge of mantle structure, composition, and processes must be augmented by geophysical remote sensing. What can these observations tell us about the major element composition of the upper mantle? How can they constrain possible differences in chemical composition between the upper and lower mantle? What light can they shed upon the nature of velocity heterogeneities in both the upper and lower mantle? It is these questions that we shall seek to address in this chapter. For brevity, we will limit the discussion to seismological and magnetotelluric studies of the mantle.

Most seismological constraints on mantle composition are derived by comparison of values of seismic wave velocities inferred for particular regions within the Earth to the values measured in the laboratory for particular minerals or mineral assemblages, with such comparisons being made under comparable regimes of pressure (P) and temperature (T). The primary parameters of interest, then, are the compressional (or P-) wave velocities (V_P) and the shear (or S-) wave velocities (V_S). These wave velocities are simply related to the density (ρ) and to the two isotropic elastic moduli, the adiabatic bulk modulus (K_S) and the shear (or 'rigidity') modulus (G), via $V_P^2 = [K_S + (4/3)G]/\rho$ and $V_S^2 = G/\rho$, respectively. Similarly, magnetotelluric studies yield estimates of electrical resistivity

(ρ_e) integrated over some range of depth. The resistivity may be compared to measured values for particular substances and the mantle's composition or state (partially molten, fluid-saturated, etc.) inferred in that depth range.

3.2.1.2 Bulk Sound Velocity

Straightforward measurements of elastic properties of materials can be made via high-pressure static compression experiments, in which X-ray diffraction (XRD) is used to measure the molar volume (V), or equivalently the density (ρ), of a material as a function of pressure (P). The pressure dependence of volume is expressed by the 'incompressibility' or isothermal bulk modulus (K_T), where $K_T = -V(\partial P/\partial V)_T = \rho(\partial P/\partial \rho)_T$.

This isothermal bulk modulus (K_T) measured by static compression differs slightly from the aforementioned adiabatic bulk modulus (K_S) defining seismic velocities in that K_T describes resistance to compression at constant temperature, such as is the case in a laboratory device in which a sample is slowly compressed in contact with a large thermal reservoir such as the atmosphere. K_S, on the other hand, describes resistance to compression under adiabatic conditions, which prevail when passage of a seismic wave causes compression (and relaxation) on a timescale that is short compared to that of thermal conduction. Thus, the adiabatic bulk modulus generally exceeds the isothermal value (usually by a few percent), because it is harder to compress a material whose temperature rises upon compression than one which is allowed to conduct away any such excess heat, as described by a simple multiplicative factor: $K_S = K_T(1 + T\alpha\gamma)$, where α is the volumetric coefficient of thermal expansion and γ is the thermodynamic Grüneisen parameter.

Experimentally, then, the bulk modulus is the simplest parameter to measure, but the seismological parameters of primary interest, V_P and V_S, both involve the shear modulus as well. It is convenient, therefore, to define a new parameter, the 'bulk sound velocity' (V_φ), which eliminates all dependence upon the shear modulus (G) through a judicious linear combination of the squares of the two seismic wave velocities: $V_\varphi^2 = K_S/\rho = V_P^2 - (4/3)V_S^2$. This new parameter (sometimes thought of as the P-wave velocity of an 'equivalent' fluid, for which $G = 0$) can be determined from dynamic (shock wave) compression data: $V_\varphi{}^2 = K_S/\rho = (1 + T\alpha\gamma)(\partial P/\partial \rho)_T$. The bulk sound velocity possesses another desirable feature in that it can also be constrained indirectly through chemical equilibrium experiments. Chemical equilibria describe free energy minima; the pressure dependence of free energy is described by the molar volume, and the pressure dependence of volume (or density) is described by K_T and hence V_φ. Thus, experimental determinations of equilibrium-phase boundaries, for example, can provide independent constraints upon V_φ (Bina and Helffrich, 1992).

Again, chemical composition in regions of the Earth's interior is primarily constrained by mapping values of seismic velocities in those regions and comparing the values to those determined for various candidate mineral assemblages. The primary observables in the seismological studies consist of measured travel times of various P- and S-waves, from a large enough set of which values of V_P and V_S can be determined through mathematical inversion. Secondary observables include the measured amplitudes of various arriving P- and S-waves, but these are much more sensitive to complex properties such as anelasticity than are simple travel times. Seismological observables, then, directly yield V_P and V_S, but static compression experiments directly yield V_φ. It is common, therefore, to seek to combine seismological V_P and V_S models to generate a V_φ model for a region, for comparison to mineralogically constrained V_φ values. Such combinatoric procedures can introduce additional errors, however, in that the V_P and V_S profiles used may often reflect seismic ray paths or frequency bands that differ from one to the other. Indeed, special source–receiver geometries (such as those whose epicentral distances are so small as to ensure nearly overlapping ray paths) may be necessary to obtain robust estimates of V_φ values (Bina and Silver, 1997). Nonetheless, comparisons to V_φ, rather than to V_P and V_S, are commonly used to constrain compositions in the deep interior, because (as noted later), mineralogical values for G (and hence for V_S) grow more problematic with increasing depth.

3.2.1.3 Acoustic Methods

Direct laboratory measurements of V_P and V_S for materials can be made through acoustic methods, such as Brillouin spectroscopy and ultrasonic techniques. Brillouin spectroscopy (or 'Brillouin scattering') determines acoustic velocities in a single crystal through measurements of the Doppler shifts experienced by visible light scattering from the interior of a single crystal in which thermally induced acoustic waves are propagating. Because the technique employs single crystals, full elasticity tensors (rather than just isotropic V_P and V_S) can be determined, which are useful in studies of velocity anisotropy. The technique requires only small samples, and because visible light is employed, the samples may be placed in an optically transparent diamond-anvil cell (DAC) in order to make measurements at elevated pressures and temperatures. DAC studies yielding V_P and V_S may be combined with XRD analyses yielding ρ, to allow for direct determination of K_S and G (and hence V_φ) for single crystals (Zha et al., 1998a).

The second group of acoustic methods, the ultrasonic techniques, require larger samples but can be performed on either single crystals or polycrystalline aggregates. They require experimental measurement (via interferometry) of the travel times of two consecutive ultrasonic echoes from the ends of a shaped sample, combined with measurement of the length of the sample. These measurements directly yield V_P and V_S, rather than full anisotropic elasticity tensors, but this is usually quite sufficient (unless patterns of seismic velocity anisotropy are to be used to map strain fields in the mantle). Samples may be placed in a DAC or a multi-anvil cell (MAC) to make measurements at elevated pressures and temperatures, and simultaneous (usually synchrotron) XRD analysis can then be used to keep track of associated changes in sample length. Again, DAC or MAC studies yielding V_P and V_S may be combined with ρ measurements from the XRD analyses to directly yield K_S and G (and hence V_φ) for samples (Li et al., 2001). Polycrystalline samples generally retain some porosity even at high pressures, which may affect the measured slopes and hence the inferred derivatives of elastic moduli, but single-crystal samples are free from such limitations.

The appealing flexibility of acoustic techniques is leading to rapid expansion of the regime of pressures and temperatures in which experimental measurements can be made. However, their potential utility continues to suffer from one poorly understood factor. While Brillouin and ultrasonic methods determine V_P and V_S at frequencies in the MHz–GHz range, seismological observations constrain V_P and V_S at frequencies in the mHz–Hz range. There is ample room for the poorly understood frequency dependence of these velocities ('dispersion') potentially to confound petrological interpretations over these many orders of magnitude. Unhappily, V_S is much more subject to dispersion than is V_P, and the magnitude of such effects upon V_S (and hence G) only grows with increasing temperature (and hence depth). Thus, until V_S values can be both measured at simultaneous high P and T and extrapolated over 12 orders of magnitude in frequency with confidence (and quantifiable error bounds), there remain important roles for the parameter V_φ. Not only does V_φ remain free of the dispersive and thermal complications of G, if determined in part by static compression methods, it also benefits from being constrained by measurements near 0 Hz, closer to the seismic frequency band than acoustic techniques permit.

3.2.1.4 Electrical Resistivity Estimation

The electrical resistivity of rocks varies over a range of 10^8. This makes the parameter a fairly sensitive probe of the mantle's constitution (Haak and Hutton, 1986; Hermance, 1995; Khan et al., 2011; Velímský, 2010a). **Figure 1** provides a sketch of resistivity values and illustrates its potential power in determining the state of the deeper mantle. Oceanic upper mantle, for example, is orders of magnitude more resistive than silicate melt. Consequently, small amounts of melt in a region of the upper mantle are detectable if its resistivity can be determined.

The magnetotelluric method is one way to estimate the resistivity of deeper parts of the Earth (Matsuno et al., 2010). Naturally occurring electrical disturbances in the ionosphere excite electromagnetic waves that perfuse the surface and elicit a response due to the subsurface resistivity. The measured values are the electrical (E) and magnetic (H) field strengths in the horizontal plane. The apparent resistivity is obtained from the off-diagonal elements Z_{xy} of the 2×2 matrix Z that relates E and H through $E = ZH$. The resistivity at frequency f is $c|Z_{xy}|^2/f$, where c is a material constant. There is a limit to the depth that an electromagnetic wave can penetrate the mantle to excite a response. The penetration depth δ is roughly given by the formula $\delta = 500\ (\rho_e/f)^{1/2}$ where δ is a value in meters if ρ_e is in ohm-m and f is in Hz. The formula shows that to penetrate conductive (low resistivity) layers, the frequencies must be low. However, because the resistivity is integrated over the whole penetration depth, it is difficult to isolate the signal to a particular depth. Thus, the resistivity profiles are best interpreted in combination with another method that has better depth resolution, like a seismological study.

3.2.1.5 Seismological Methods: Velocity Contrasts

Seismology constrains velocity contrasts through observations of P- and S-wave travel times or by seismic wave amplitudes. Mathematical inversion of large numbers of travel times, observed at a variety of distances between source (earthquake) and receiver (seismometer), results in velocity profiles that represent the variation of V_P and V_S (or V_φ) as functions of depth. The changes in velocities across seismic 'discontinuities' in these models can then be compared to the velocity changes across phase changes in olivine, as calculated from laboratory data, in order to estimate mantle olivine content. Unfortunately, seismic velocity profiles determined from such inversions generally are not very sensitive to, and therefore do not well constrain, the magnitudes of velocity discontinuities. This is especially true of globally averaged seismic velocity models. Local or regional studies that include travel times and/or amplitudes of special seismic arrivals that have interacted directly with (been reflected or undergone P–S conversions at) the seismic discontinuities are best able to provide such constraints (Lay and Garnero, 2011).

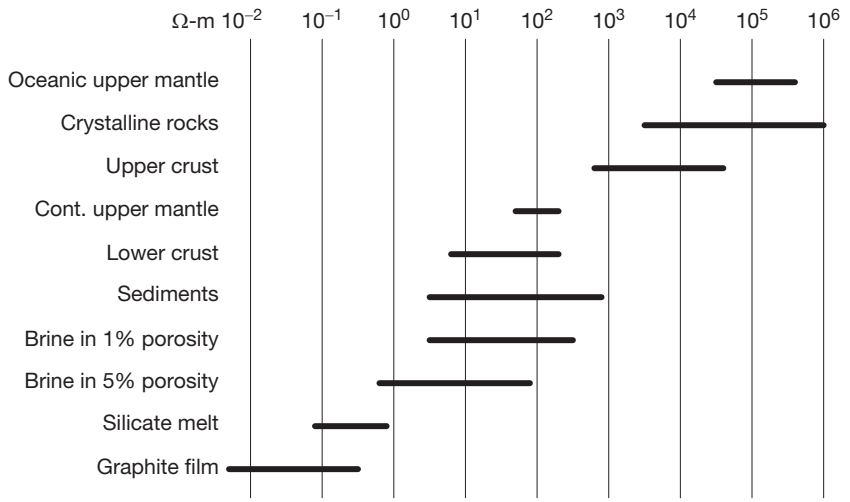

Figure 1 A sketch of resistivity values illustrating its potential power in determining the state of the deeper mantle. Resistivity varies over eight orders of magnitude in mantle rocks, whereas seismic wave speeds vary only by about a factor of 2. Redrawn from Haak V and Hutton VSR (1986) Electrical resistivity in continental lower crust. In: Dawson JB, Carswell DA, Hall J, and Wedepohl KH (eds.) *The Nature of the Lower Continental Crust*, *Geological Society Special Publication* 24, pp. 35–49. London: Geological Society of London, with permission from the Geological Society of London.

3.2.1.6 Seismological Methods: Differential Travel Times

Specific types of seismic studies that use differential travel times, as opposed to absolute travel times, are more robust to the influence of unusual structure near either the earthquake source or the receiver (Lay and Garnero, 2011). One example of this type is receiver function studies that use the time lag between the direct P-wave arrival and the P-to-S converted wave from a discontinuity that lags direct P. Another example is precursor studies that use the arrival times of waves reflected from the underside of a seismic discontinuity to determine their depths by comparison with a reflection from the surface. The time lag between the precursory arrival and surface arrival provides the depth. A final example comprises converted- or scattered-wave studies from earthquakes. The earthquake emits both P- and S-waves. If the S-wave converts to P at a discontinuity below the earthquake or at a scatterer in the earthquake's vicinity, the later arrival's time lag relative to P provides the location of the conversion or scattering point. Figure 2 shows typical geometries.

3.2.1.7 Seismological Methods: Spatial Localization of the Signal

Different study types lead to different location methods for the velocity changes that produce observable effects on the seismic wavefield. The receiver function geometry in Figure 2 shows that the signal originates below the station, closer to the receiver than the source. While the origin is clear, the study locations are restricted to lie near the seismic station. Most stations being on land, and most land being in the northern hemisphere, this means that much of the Earth's subsurface cannot be studied with receiver functions. Similarly, near-source conversion or scattering studies only illuminate structure near the earthquakes themselves. The aseismic continental interiors are thus unsuitable targets of such studies. In contrast, the underside bounce geometry provides worldwide coverage subject to the limitations of the paths that seismic waves take between earthquakes and seismic stations.

Underside bounce geometries have the peculiar feature that the observed arrival is the slowest way that a reflected seismic wave can reach a particular station. All the other earlier arrivals are canceled out by mutual destructive interference. If the seismic structure along all of the destructively interfering paths is not uniform, the observed ray will emanate from elsewhere than the expected bounce point, mapping the signal to the wrong place. Consequently, a trade-off exists between coverage and spatial signal fidelity.

3.2.1.8 Seismological Methods: Density Constraints

Though density and seismic wave speed are related through the nature and strength of the chemical bonds making up a mineral, seismology provides few direct constraints on density. The principal one is from the vibrational modes of the whole Earth when it is set in motion by large earthquakes. The modes that swell and shrink the size of the Earth are sensitive to gravity and therefore to the radial density structure. The vibrations have very low frequencies and, consequently, very long wavelengths. Thus, the density constraints they provide are average densities through a depth range rather than specific density values at particular depths. The nature of the constraints is such that the more specific the depth, the more uncertain is the density.

The amplitudes of seismic wave reflections generally are sensitive to the impedance change across the reflective discontinuity. Impedance is the product of wave speed and density. Thus, amplitudes constrain local changes in density (if wave speeds are known independently) but not their absolute value.

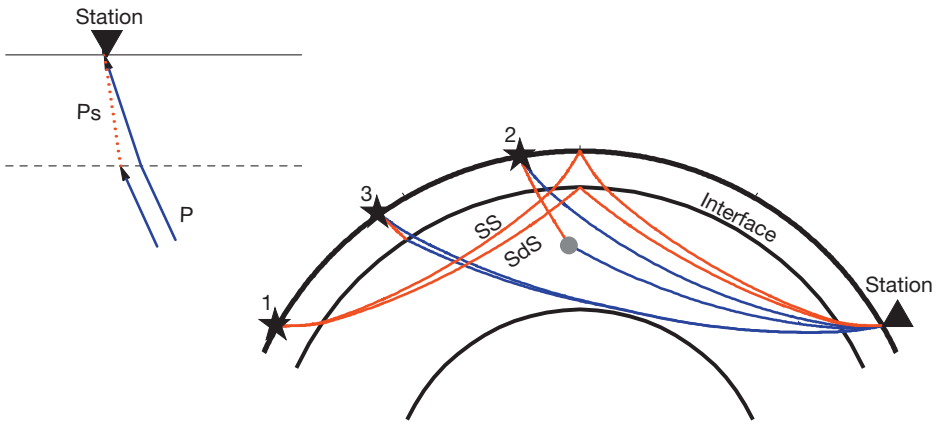

Figure 2 Example paths encountered in differential travel time studies. Stars indicate earthquakes and triangles indicate a seismic station. P waves are blue, and S waves are red. A receiver function study (left) uses the lag between the direct P wave arrival (solid line) and a P-to-S conversion from an interface (Ps, dotted line) to infer the layer depth and properties. The time lag after the P arrival and its amplitude relative to P provide the main observables for analysis of a local structure near the station. Underside discontinuity studies (right, 1) use the lag between SdS (an earlier-arriving shear-wave reflection from beneath the interface) and SS (a reflection from the surface) to infer the depth to the interface. A scatterer in the deep mantle (gray spot) illuminated by an S wave from the source (2) that converts to P at the scatterer is located partly using the time lag after the direct P wave (solid line). The depth to an interface close to the source can be determined (3) from the lag between the S wave from the source that converts to P at the interface and the direct P wave.

3.2.1.9 Seismological Methods: Scattering

Seismic wave scattering arises when there is a contrast in material properties over spatial scales that is substantially shorter than a seismic wavelength. With changes this abrupt, the material behaves as if it is a new, but weaker seismic energy source, radiating waves omnidirectionally. The path a scattered wave takes is not ray-like. Locating scatterers spatially requires many observations (Kaneshima and Helffrich, 2010).

It also requires the weak arrival to be recognizable. If it arrives too close to a wave directly emanating from the earthquake, detection is impossible. Consequently, scatterers close to earthquakes, near direct ray paths, or in strongly attenuating regions, are difficult to observe. This generally excludes the upper mantle from study using scattering.

3.2.1.10 Seismological Methods: Tomography

Tomographic imaging provides a compelling way to visualize the Earth's structure by processing enormous volumes of local and distant earthquake travel-time data. The more detailed the image, the more data are required to resolve the values in each image pixel. In geophysical applications, there is rarely enough constraining data. Thus, additional constraints must be recruited to achieve sensible results.

The most common constraint is the belief that the minimum structure required to fit the data within its observational uncertainty should be inferred. This leads to bland looking images rather than dramatic ones with sharp boundaries and large wave speed contrasts. It does not mean that the image is free of such contrasts, but merely that they are suppressed by philosophical and practical necessity. However, interpreting images requires one to know how much structural suppressing is used (Lay and Garnero, 2011).

Furthermore, it is important to bear in mind that tomographic images depict wave speeds relative to a selected reference model, thereby complicating the extraction of absolute velocities. A given depth range below a particular geographic region, for example, may appear to be either very fast, moderately fast, or slow, depending upon the particular reference model chosen to address a particular geophysical question.

3.2.2 Upper Mantle Bulk Composition

3.2.2.1 Overview

Based upon the compositions of mantle rocks emplaced at the surface in large slices (**Chapter 3.4**) or as small xenoliths (**Chapter 3.5**), the compositions of mantle-derived melts (**Chapter 3.3**), various cosmochemical arguments (**Chapters 3.1** and **3.16**), and simple geophysical considerations, the mineralogy of the upper mantle is commonly concluded to resemble that of some sort of peridotite (McDonough and Rudnick, 1998). Perhaps the most frequently invoked model composition is that of 'pyrolite' (Ringwood, 1975, 1989), which contains about 60% olivine by volume, the depth-varying properties of which are dominated by progressive high-pressure phase transitions from olivine (α) to wadsleyite (β, formerly called 'modified spinel') to ringwoodite (γ, formerly called 'silicate spinel'), and thence to a mixture of silicate perovskite (pv) and magnesiowüstite (mw, also called 'ferropericlase', fp). The remaining, non-olivine, components are orthopyroxene (opx), clinopyroxene (cpx), and garnet (gt), and these undergo more gradual high-pressure transitions as the pyroxenes dissolve into the garnet, with the resulting 'garnet-majorite' solid solution (gt-mj) eventually transforming to silicate perovskite as well (**Figure 3**). While this model of a peridotitic upper mantle has regularly been challenged, the proposed alternatives have evolved over time to accommodate increasing quantities of olivine: from an eclogite containing little or no olivine (Anderson, 1979, 1982, 1984), through various picritic eclogite or 'piclogite' models containing 16% (Bass and Anderson, 1984), 22% (Anderson and Bass, 1984), 30% (Anderson and Bass, 1986), or 40% (Duffy and Anderson, 1989; Duffy et al., 1995) olivine. Thus, 'pyrolite' and 'piclogite' represent broad families of mantle compositions that are distinguished primarily by the former having >50% olivine by volume and the latter having <50% olivine.

Estimates of a suitable peridotite composition have also varied: from 40–70% olivine (Weidner, 1986) to 66–74% (Bina and Wood, 1987), for example. Indeed, for several years, these two end-member models seemed to be converging toward 50% olivine (Agee, 1998; Ita and Stixrude, 1992; Jeanloz, 1995; Shearer and Flanagan, 1999). As the arguments hinge upon comparisons of seismic wave velocities in the upper mantle with velocity profiles computed for candidate mineral assemblages, firmer constraints upon this number require not only better experimental measurements of the simultaneous dependence of the elastic properties of mineral assemblages upon both temperature and pressure (Sinogeikin et al., 1998; Zha et al., 1998b) but also increased seismological resolution of the laterally varying velocity contrasts at depth within the upper mantle (Melbourne and Helmberger, 1998).

Both such peridotite and piclogite models of mantle bulk composition generally presume that coexisting minerals are in local chemical equilibrium. However, it has long been suggested that some minerals, such as silica phases in basalts, may survive as disequilibrium assemblages during subduction into the mantle (Bina, 2003; Ganguly et al., 2009; Kaneshima and Helffrich, 1999; Niu et al., 2003; Ricard et al., 2005; Ringwood and Irifune, 1988), given the slow chemical diffusion rates thought to prevail at depth in the absence of fluids or melts. More recently, this has led to the proposal (Stixrude and Lithgow-Bertelloni, 2012; Xu et al., 2008) that much or all of the mantle may potentially consist of disequilibrium mechanical mixtures of peridotite and recycled subducted slab material in the form of eclogite and harzburgite. (Unfortunately, such a mechanical mixture of peridotite and eclogite is sometimes also referred to as 'piclogite' (Bianchini et al., 2010), potentially sowing confusion.) It is argued that such a mechanical mixture can provide a better fit to the fine structure of seismic velocities in the transition zone than equilibrium assemblages. However, both mechanical mixtures and equilibrium assemblages along 1600 K adiabats are found to be slightly faster than reference seismological models in the upper mantle and slightly slower in the lower mantle, suggesting either enrichment in the basaltic component of the lower mantle relative to the upper mantle or deviation of the geotherm from the chosen model adiabat (Stixrude and Lithgow-Bertelloni, 2010).

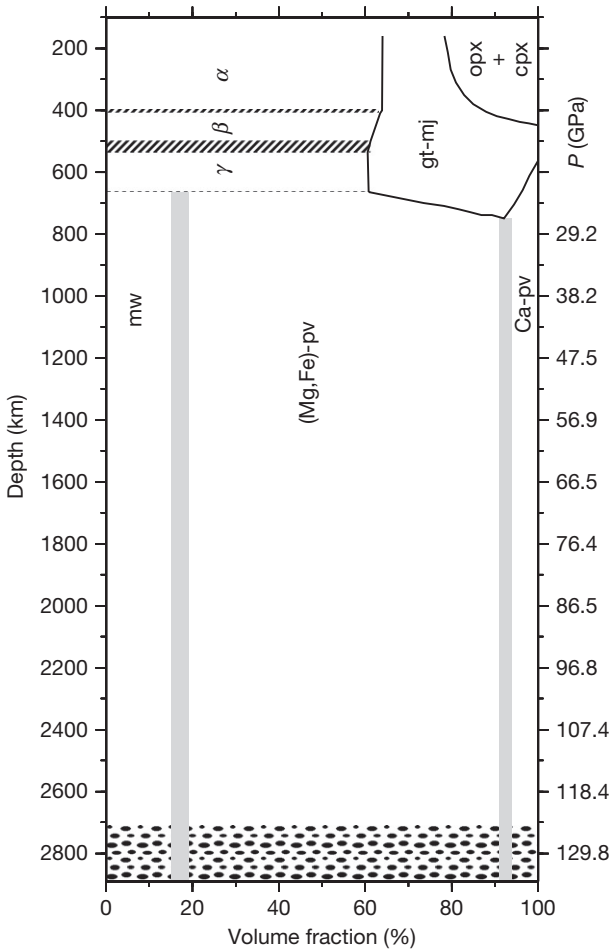

Figure 3 Depth-varying phase proportions in a pyrolite mantle (after manner of Ringwood, 1989). Phases are: (α) olivine, (β) wadsleyite, (γ) ringwoodite, (opx) orthopyroxene, (cpx) clinopyroxene, (gt-mj) garnet-majorite, (mw) magnesiowüstite, ([Mg,Fe]-pv) ferromagnesian silicate perovskite, and (Ca-pv) calcium silicate perovskite. Patterned region at base denotes complexity and heterogeneity near the core–mantle boundary.

3.2.2.2 Velocity Contrasts

Seismological methods such as receiver function studies and underside reflections provide estimates of velocity contrasts across the discontinuities that convert or reflect seismic waves. The range dependence of travel time triplications also yields discontinuity contrasts. The changes in velocities across seismic 'discontinuities' in these models can then be compared to the velocity changes across phase changes in olivine, as calculated from laboratory data, in order to estimate mantle olivine content. Unfortunately, seismic velocity profiles determined from such inversions generally are not very sensitive to, and therefore do not well constrain, the magnitudes of velocity discontinuities, especially true of globally averaged seismic velocity models. Local or regional studies that include travel times of special seismic arrivals that have interacted directly with (been reflected or undergone P–S conversions at) the seismic discontinuities are best able to provide such constraints.

Recent measurements of elastic wave velocities in olivine, wadsleyite, and ringwoodite at high pressures and temperatures (Irifune et al., 2008; Li and Liebermann, 2007; Li et al., 2001) suggest reasonable consistency between a standard pyrolite model containing about 60% olivine and high-resolution seismic velocity profiles of the transition zone, especially if some degree of hydration is taken into account (Mao et al., 2008). On the other hand, a study (Cammarano and Romanowicz, 2007) using long-period seismic waveforms to invert for absolute velocities as perturbations relative to mineralogical (rather than seismological) reference models yielded both a slower transition zone and a faster shallow upper mantle than estimated for homogeneous dry pyrolite, which would be consistent with some combination of hydration and a gradual increase in garnet (piclogitic) component with depth, and slow velocities at the base of the transition zone determined from triplications beneath Tibet (Zhang et al., 2011) have led to similar inferences. Arguments about $\pm$5% olivine aside, however, we can perhaps safely refer to the upper mantle as a peridotite, as the International Union of Geological Sciences (IUGS) classification of ultramafic rocks defines a peridotite as containing 40% or more olivine.

3.2.2.3 Discontinuity Topography

Perhaps one of the most important consequences of a peridotite composition for the upper mantle is that the phase

transitions in olivine that are manifested as seismic discontinuities should exhibit thermally controlled variations in their depth of occurrence that are consistent with the measured Clapeyron slopes (Bina and Helffrich, 1994) of the transitions. In particular, the olivine–wadsleyite transition at 410 km should be deflected upward in the cold environment of subduction zones while the disproportionation of ringwoodite to silicate perovskite and magnesiowüstite at 660 km should be deflected downward, thereby locally thickening the transition zone. In anomalously warm regions (such as the environs of mantle plumes as described below), the opposite deflections at 410 and 660 km should locally thin the transition zone. The seismically observed topography of 20–60 km on each of the 410 and 660 is consistent with lateral thermal anomalies of 700 K or less (Helffrich, 2000; Helffrich and Wood, 2001).

Other consequences of thermally perturbed phase relations in mantle peridotite (**Figure 4**) are also supported by seismological observations. These include anticorrelation of transition zone thickness and transition zone delay times, whereby positive delays in travel times, which imply slow velocities (and therefore high temperatures), are observed to correlate with negative changes in (thinning of) transition zone thickness (Gu and Dziewonski, 2002; Lebedev et al., 2002). Similarly, observations of anticorrelation of transition zone thickness and depth to the 410 km discontinuity are consistent with thermal deflection of phase boundaries, as a positive increase in transition zone thickness (implying low temperatures) correlates with a negative change in depth to (implying uplift of) the 410 (Li et al., 2003). Furthermore, seismological observations suggest the presence of a thicker (colder) transition zone under continents than under (warmer) oceans (Gu and Dziewonski, 2002), as well as a thicker transition zone beneath (colder) subduction zones than beneath the (warmer) mid-Pacific (Gu and Dziewonski, 2002; Houser et al., 2008).

Evidence for the expected anticorrelation of topography on the 410 and the 660, whereby one may be expected to deflect upward in any locale where the other deflects downward, has been less robust than these other observations (Gilbert et al., 2003; Helffrich, 2000; Houser et al., 2008; Lawrence and Shearer, 2008). This might arise because the assumption of vertically coherent thermal anomalies is invalid (or there may be no thermal anomalies in the regions studied). Anticorrelation may be obscured by the dependence of absolute depth estimates upon assumptions about shallower velocity structures. Clear anticorrelation of 410 and 660 topography may also be confounded by frequency-dependent effects (Helffrich, 2000; Helffrich and Bina, 1994): while the 660 may remain sharp in both cold and warm environments, the 410 should grow sharper in warm regions and more diffuse in cold regions, so that these two discontinuities may respond differently to seismic waves of different wavelengths at different temperatures. Overall, however, the bulk of the observational evidence indicates that topography on seismic discontinuities in the transition zone is caused by thermal perturbations of equilibrium phase transformations in a mantle of peridotite composition (Helffrich and Wood, 2001).

3.2.2.4 Sharpness

Other arguments about the composition of the transition zone have focused specifically upon the observed seismic 'sharpness' or depth extent of the 410 km discontinuity, which sometimes appears to occur over a narrower depth interval than might be expected for the olivine–wadsleyite phase transition. A number of phenomena have been invoked to explain apparent variations in transition sharpness, including kinetic effects on phase transformations (Solomatov and Stevenson, 1994), whereby low-pressure phases persist metastably for a finite extent before abruptly transforming to the stable high-pressure phases, thus eliminating what might otherwise be a finite mixed-phase regime, as well as probable nonlinearity of multivariant phase changes (Helffrich and Bina, 1994; Stixrude, 1997), whereby a gradual transition appears seismically to be sharper because a large fraction of the associated velocity change is concentrated within a particular portion of the mixed-phase regime. Differential solubility of water within minerals across phase changes (Helffrich and Wood, 1996; Smyth and Frost, 2002; Wood, 1995) can also affect transition sharpness, in that small amounts of dissolved H_2O should broaden the $\alpha \rightarrow \beta$ transition at 410, while an excess of H_2O resulting in a free fluid phase may be expected to sharpen the same transition. Because the sharpness of the 410 may be particularly sensitive to water, recent studies have begun to attempt to map water contents in the transition zone by examining the manner in which its sharpness appears to vary as a function of the frequency (and hence wavelength) of the interacting seismic waves (van der Meijde et al., 2003).

Studies of multiphase Mg–Fe partitioning between coexisting olivine, wadsleyite, pyroxene, and garnet have also suggested that such partitioning can act to sharpen the $\alpha \rightarrow \beta$

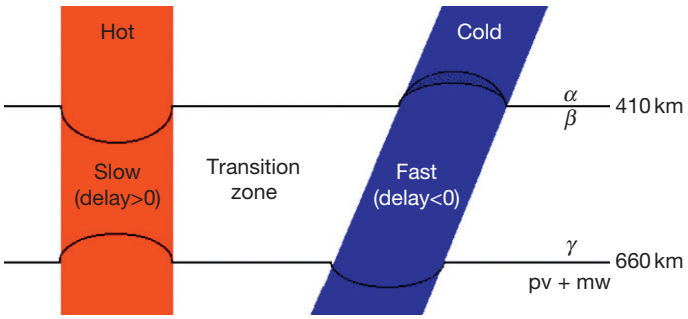

Figure 4 Schematic illustration of thermal control of olivine phase transformations in the transition zone, showing perturbations to transition zone thickness, transition zone seismic velocities (delay times), and depths of individual phase transformations.

transition at 410 (Irifune and Isshiki, 1998). It is somewhat ironic that the non-olivine phases that exhibit a very broad pyroxene–garnet transition can, nonetheless, induce the already sharp olivine–wadsleyite transition to grow yet sharper simply by slightly shifting the effective Mg/Fe ratio in olivine through cation exchange. Additional multiphase studies (Frost, 2003) have concluded that the entire range of seismically inferred 410 km transition widths can be explained by the combined effects of such elemental partitioning, nonideal mixing, temperature variations, and hydration on the $\alpha \rightarrow \beta$ transition in a peridotite mantle composition.

3.2.2.5 Broadening and Bifurcation

As noted, low temperatures alone can serve to broaden the 410 by expanding the depth extent of the $\alpha+\beta$ mixed-phase stability field (Bina and Helffrich, 1994; Katsura and Ito, 1989;). Even more confusingly, however, low temperatures can give rise to bifurcation of the $\alpha \rightarrow \beta$ transition (Figure 5), resulting in a strongly uplifted $\alpha \rightarrow \alpha+\gamma$ transition, which is seismically diffuse, overlying a less strongly uplifted $\alpha+\gamma \rightarrow \alpha+\beta$ or $\alpha+\gamma \rightarrow \beta+\gamma$ transition, which is seismically sharp (Bina, 2003; Green and Houston, 1995; Vacher et al., 1999). As a result, α still transforms to β (and eventually to γ), but it does so by a two-step process, and whether a strongly uplifted broadened transition or a weakly uplifted sharpened transition is observed may depend upon the frequency of the interacting seismic waves. While understanding of such sharpening and broadening processes may be important for resolving fine details of the thermal structure of the transition zone, they would seem to have less bearing upon the overall bulk chemistry of the upper mantle, with the possible exception of constraints on local volatile contents (Wood et al., 1996).

However, within the cold environment of subduction zones, the temperature dependence of phase relations in olivine near depths of 410 km does exhibit particular sensitivity to bulk Mg/(Mg+Fe) ratios. Indeed, the effect on olivine phase relations of Fe enrichment is largely analogous to

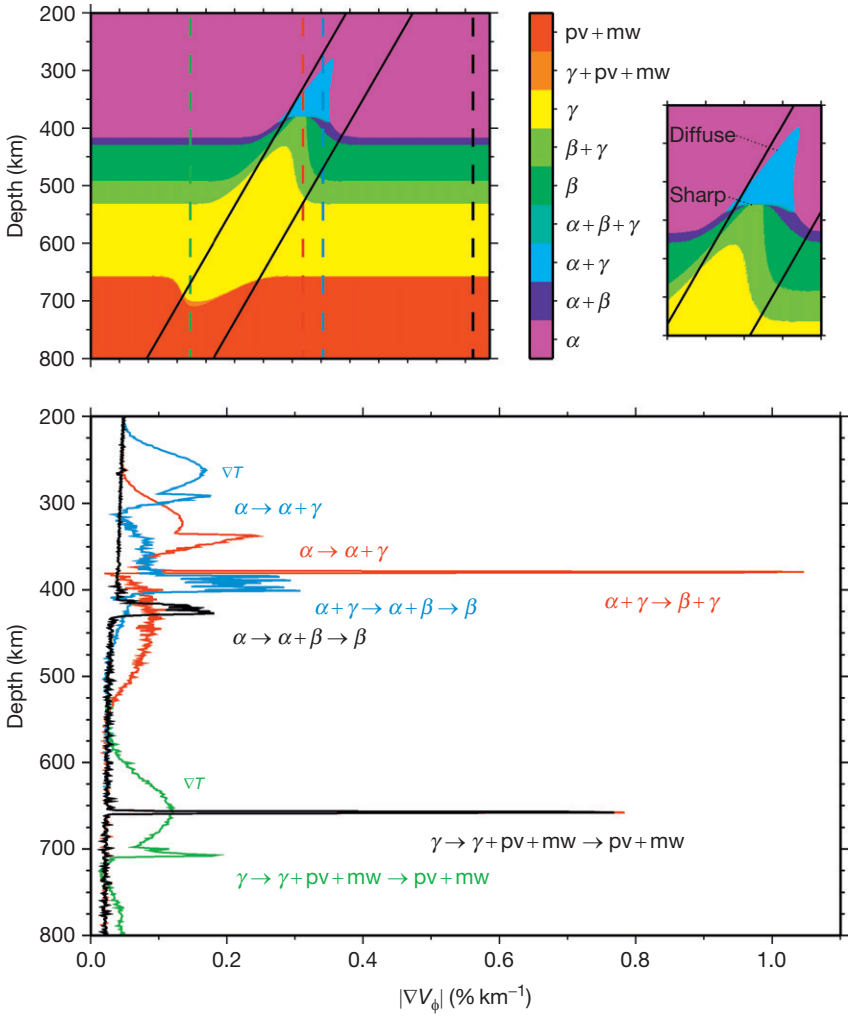

Figure 5 Effects (top) upon olivine phase equilibria of low temperatures in subduction zones. Dark lines denote slab boundaries. Phases are olivine (α), wadsleyite (β), ringwoodite (γ), magnesiowüstite (mw), and ferromagnesian silicate perovskite (pv). Note (inset) that the $\alpha \rightarrow \beta$ transition near 410 km is first uplifted and then bifurcates into a strongly uplifted diffuse $\alpha \rightarrow \alpha+\gamma$ transition overlying a weakly uplifted sharp boundary (after Bina, 2003). Corresponding velocity gradients (bottom) are plotted for four vertical sections (colored dashed lines from top left panel). Sources of steep gradients are labeled with corresponding phase transitions or a steep temperature gradient at upper slab surface (∇T). Vertical resolution is 1 km.

that of lower temperatures noted earlier. For pyrolitic values (Mg/(Mg+Fe)=0.90), equilibrium phase relations (Fei et al., 1991) predict uplift and broadening of the sharp $\alpha \rightarrow \beta$ transition in the cold slab, replacement of the sharp $\alpha \rightarrow \beta$ transition by a more diffuse $\alpha \rightarrow \alpha+\gamma$ transition overlying a sharper $\alpha+\gamma \rightarrow \alpha+\beta$ or $\alpha+\gamma \rightarrow \beta+\gamma$ transition within the colder interior of the slab, and uplift of the broad $\beta \rightarrow \beta+\gamma \rightarrow \gamma$ transition (Figures 5 and 6); this is equivalent to the bifurcated scenario discussed earlier for low temperatures. Further Mg enrichment (Mg/(Mg+Fe)=0.99) would result in smaller uplift of a sharper $\alpha \rightarrow \beta$ transition, little or no replacement of the sharp $\alpha \rightarrow \beta$ transition by a more diffuse $\alpha \rightarrow \alpha+\gamma$ transition within the cold interior of the slab, and an uplifted $\beta \rightarrow \gamma$ transition which is much sharper within both the slab and the ambient mantle; such sharpening is analogous to the effect of slightly warmer temperatures. This latter scenario would also correspond to a globally sharp 520 km discontinuity, as well as a globally sharp 410 km discontinuity, which remains sharp when uplifted (Figure 6). On the other hand, Fe enrichment (Mg/(Mg+Fe)=0.81) would result in complete replacement of the sharp $\alpha \rightarrow \beta$ transition within both the slab and the ambient mantle by a more diffuse and strongly uplifted $\alpha \rightarrow \alpha+\gamma$ transition overlying a sharper $\alpha+\gamma \rightarrow \alpha+\beta \rightarrow \beta$ or $\alpha+\gamma \rightarrow \beta+\gamma$ transition, as well as further broadening of the uplifted $\beta \rightarrow \beta+\gamma \rightarrow \gamma$ transition; this would be equivalent to the effect of very low temperatures. Such a scenario would correspond to a globally very diffuse 520 km discontinuity and a 410 km discontinuity consisting of a broad velocity gradient overlying a sharp velocity jump (Figure 6).

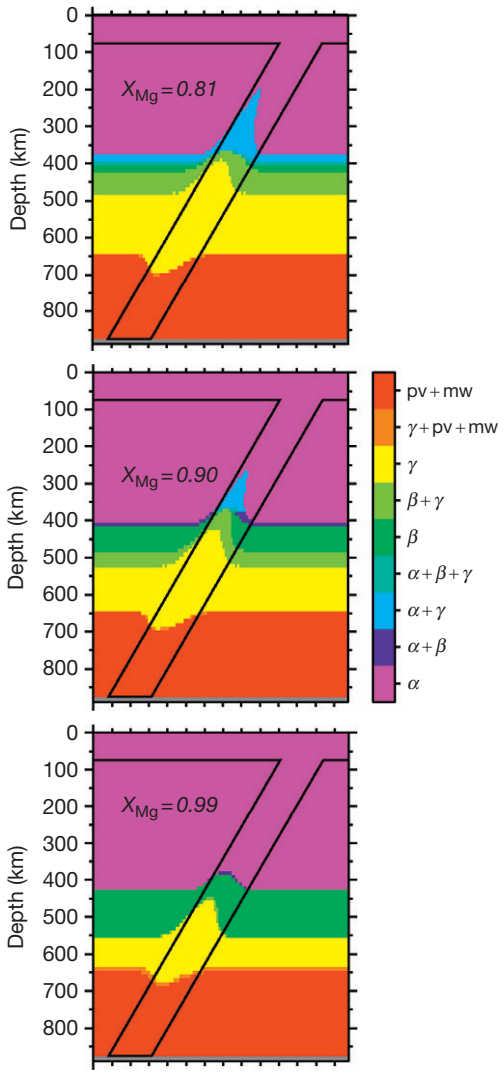

Figure 6 Effects upon olivine phase equilibria of variations in Mg/(Mg+Fe) for pyrolite (center), Fe enrichment (top), and Mg enrichment (bottom). Vertical resolution is 10 km.

Other complexities of transition zone seismic structure may also indicate thermal or compositional effects. Apparent bifurcation of the 520 into superposed 500 and 550 km discontinuities (Deuss and Woodhouse, 2001) could reflect distinct signatures of the $\beta \rightarrow \beta+\gamma \rightarrow \gamma$ transition and exsolution of calcium silicate perovskite from majoritic garnet (Figure 3), and the offset in depth between these two features might also be expected to change with temperature. Moreover, in colder regions majoritic garnet may transform to akimotoite (formerly known as silicate ilmenite, ilm), within the 550–600 km depth range, prior to eventual disproportionation to silicate perovskite and magnesiowüstite, but this interposed gt→ilm transition is unlikely to express a significant seismic velocity signature, at least not within subducting slabs (Vacher et al., 1999).

Furthermore, the sharp $\gamma \rightarrow$ pv+mw transition near 660 km and the broader gt→pv transition which proceeds to completion at somewhat greater depths may be offset by amounts that vary with temperature and composition, and some seismological studies (Ai et al., 2003; Andrews and Deuss, 2008; Deuss et al., 2006; Simmons and Gurrola, 2000) have suggested just such multiple discontinuities near 660 km and below. However, other detailed analyses using receiver functions (Lawrence and Shearer, 2006; Thompson et al., 2011) reveal no evidence of such discontinuity multiplicity. This suggests that low-amplitude energy arriving after P-to-S conversions at 660 km may be the result of reverberations from shallower discontinuities or a methodological artifact.

Overall, seismological observations of a sharp 410 km discontinuity, which is occasionally broader in places, which exhibits topography anticorrelated with that observed on the sharper 660 km discontinuity (Lawrence and Shearer, 2008), and which may be accompanied by a sporadic 520 km discontinuity (Gu et al., 1998; Li, 2003), are primarily consistent with pyrolitic Mg/(Mg+Fe) values of 0.90, but local variations certainly cannot be excluded.

3.2.3 Upper Mantle Heterogeneity

3.2.3.1 Subducted Basalts

The fate of the basalts and gabbros in the oceanic crust as they are subducted into a peridotite upper mantle can also be studied using seismological methods. Anhydrous metabasalts may be expected to undergo equilibrium transformation to an eclogite assemblage (with growth of garnet at the expense of plagioclase) around depths of 20–50 km (Hacker, 1996; Peacock, 1993; Wood, 1987). Such eclogites should be about 2% faster than surrounding pyrolite at depths of about 280 km

(Helffrich and Stein, 1993; Helffrich et al., 1989). However, most of this velocity contrast arises solely from the temperature contrast between cold slab (1000 °C at 9.6 GPa) and warmer mantle, with the composition difference alone giving rise to a contrast of only about 0.5% (Helffrich et al., 1989). Consideration of silica-oversaturated basalt compositions can expand this range of velocity contrasts somewhat, with anhydrous coesite eclogites being about 2–4% faster and, subsequent to the transition from coesite to stishovite at around 220–240 km depth, stishovite eclogites being about 4–6% faster (Connolly and Kerrick, 2002). Again, however, it is important to bear in mind that much of this contrast arises due to low slab temperatures alone, so that thermally equilibrated eclogites lingering long in the upper mantle would appear only slightly (if at all) faster relative to ambient mantle.

In large part, this ability of anhydrous basaltic eclogites to seismically blend into an ultramafic mantle arises from the behavior of elastic moduli in pyroxenes. In the shallowest upper mantle, orthopyroxene is about 6% slower in V_P relative to olivine and about equal in V_S. However, the bulk modulus of orthopyroxene exhibits a strong and nonlinear increase with pressure, so that there is little significant difference in either V_P or V_S between orthopyroxene and olivine by about 200 km depth (Flesch et al., 1998; James et al., 2004). This absence of effective velocity contrasts between anhydrous eclogites and mantle peridotites within most of the upper mantle (Helffrich, 1996; Helffrich et al., 1989) is also evident in the observation that model upper mantles of both pyrolite (~60% olivine) and piclogite (~40% olivine) composition exhibit similar velocities over the 100–400 km depth range (Vacher et al., 1998).

If anhydrous metabasalts in an eclogite assemblage can generate only small fast-velocity anomalies or no anomalies at all, then a puzzle emerges in understanding subduction zone structures. Seismological observations in Japan, Tonga, Alaska, and other active subduction zones demonstrate the presence of 4–10% slower velocities in a layer 2–10 km thick along the upper surfaces of subduction zones in the depth range 100–250 km (Connolly and Kerrick, 2002; Helffrich, 1996; Kawakatsu and Watada, 2007). One explanation that has been advanced to explain the presence of such low-velocity layers involves kinetic hindrance in cold slabs. Rather than equilibrium transformation of slow anhydrous gabbro to fast eclogite at depths of 20–50 km, a model of metastable persistence of gabbro in the blueschist and eclogite stability fields, perhaps below 100 km depth, has been invoked (Connolly and Kerrick, 2002; Hacker, 1996). However, it appears that this model of metastable anhydrous gabbro may not be appropriate (Helffrich, 1996), not only because oceanic basalts commonly are found to be hydrothermally altered but also because metastable gabbro appears to be too slow seismically (Connolly and Kerrick, 2002).

Indeed, hydrothermal alteration of basalts may be a key to understanding the low-velocity layers in subducting slabs. In hydrous metabasalts under subduction zone conditions, lawsonite blueschist is expected to be the initially dominant facies (Peacock, 1993). At 65 km depth in subducting basaltic crust, lawsonite blueschist would be about 7% slower than the overlying peridotite mantle and about 8% slower than the underlying garnet harzburgite layer of the subducting lithosphere, suggesting that hydrous metabasalts may be the cause of the seismologically detected low-velocity layers (Helffrich, 1996). As hydrous gabbroic crust subducts beyond the blueschist regime, the resulting equilibrium lawsonite eclogites should still be 3–7% slower (Connolly and Kerrick, 2002). With continued subduction, garnet increases and lawsonite decreases in abundance, until the coesite–stishovite transition near 220–240 km further destabilizes lawsonite, giving rise to stishovite eclogites, which should be 4–6% faster (Connolly and Kerrick, 2002). Such a change from slow lawsonite eclogites or coesite eclogites to fast stishovite eclogites is consistent with the observed termination of low-velocity layers and, indeed, with the occasional presence of high-velocity layers, below 250 km depth. Progressive dehydration of a subducting slab may also transfer water to the mantle overlying the slab, potentially serpentinizing it. Kawakatsu and Watada (2007) propose such a model based on a change in the sign of the velocity contrast as the Pacific Plate is subducted under Japan. Here, the dominant change in velocity occurs on the mantle side of the slab/mantle interface rather than in the mineralogy of the slab itself.

Interestingly, a dominant role for lawsonite eclogites in subducting oceanic crustal material may be echoed in the occurrence of lawsonite (or pseudomorphs thereafter) among the glaucophane eclogites of the Alpine Sesia zone, a complex of continental provenance presumably exhumed after subduction to at least 60 km depth (Pognante, 1989; Reinsch, 1979). Furthermore, the compositions of majoritic and sodium-rich garnets occasionally found as inclusions in diamonds are also consistent with equilibrium phase relations for basaltic crust which has penetrated into the transition zone (Ono and Yasuda, 1996). Within the transition zone, evidence from seismic tomography suggests that some subducting slab material penetrates directly into the lower mantle while, in other subduction zones, some is deflected horizontally at depths shallower than 1000 km (Fukao et al., 2001, 2009; Takenaka et al., 1999). By the time subducted basaltic material enters the lower mantle, it may be largely dehydrated and should adopt a simpler, high-pressure perovskitite mineralogy. The expected seismic signatures of such basaltic material in the lower mantle will be examined in a later section.

3.2.3.2 Subduction-Introduced Volatiles

As subducting slabs sink from the surface into the mantle, they are likely to transport volatiles (e.g., H_2O, CO_2) into the deeper mantle (Litasov and Ohtani, 2007; Wood et al., 1996). Water is certainly transported into the upper mantle, as demonstrated by arc volcanism and by seismological evidence (Kawakatsu and Watada, 2007) for hydration–dehydration reactions along the slab surface to depths of at least 150 km. Furthermore, potential mineralic hosts for OH remain stable throughout the transition zone and into the lower mantle, suggesting that volatiles may be transported well below 700 km depth (Ohtani, 2005). However, there remains debate over the maximum depth to which such volatiles may be transported. Much of the argument centers around recent seismic observations (Jiang et al., 2008; Kaneshima et al., 2007; Kawakatsu and Yoshioka, 2011) interpreted as evidence for metastable persistence of olivine (Kubo et al., 2004; Mosenfelder et al., 2001)

into the transition zone. Measurements of the effect of water upon transformation kinetics suggest that metastable persistence of olivine should only occur in largely dry rocks (Hosoya et al., 2005). As a result, Green et al. (2010) have argued that, if much intermediate-depth and deep seismicity is caused by transformational faulting mechanisms involving metastable olivine (Green and Houston, 1995; Kirby et al., 1996), then the occurrence of such seismicity coupled with seismological observation of metastable olivine requires slabs to be dry by the time they enter the transition zone. Of course, it may be that transformational faulting is not the dominant mechanism for deep seismogenesis. Moreover, to satisfy observational constraints, only the coldest part of the slab interior, where metastable persistence is most likely to occur, need be dry. The shallower parts of the slab, which are most likely to have been hydrated through hydrothermal activity or sedimentary diagenesis, may continue to transport volatiles.

Other geophysical evidence for deepwater transport includes observation of apparent broadening of the 410 km seismic discontinuity (van der Meijde et al., 2003), an effect expected due to OH-partitioning relations between olivine polymorphs (Helffrich and Wood, 1996; Ohtani and Litasov, 2006; Smyth and Frost, 2002), along with reports of high electrical conductivity of the upper mantle above the transition zone (Tarits et al., 2004).

Furthermore, it has been suggested that reports of zones of low seismic velocity on top of the 410 km discontinuity (Hier-Majumder and Courtier, 2011; Jasbinsek and Dueker, 2007; Schaeffer and Bostock, 2010; Song et al., 2004; Tauzin et al., 2010) may be due to partial melting arising from differential water solubility between olivine and wadsleyite at 410 km (Bercovici and Karato, 2003; Hirschmann, 2006). However, other studies report no robust observation of such low-velocity zones (Thompson et al., 2011), and the question of the potential gravitational stability of such melts remains an active area of experimental investigation (Matsukage et al., 2005; Sakamaki et al., 2006). Additional problems with the melt model revolve around the geochemical imprint on the upper mantle that would result. First, melting in the presence of garnet leads to a key diagnostic of melting depth (Hirschmann and Stolper, 1996). The variable enrichment in rare earth elements (REE) of solids in the upper mantle is used to detect the depth of melting via garnet presence (HREE-enriched) or absence (REE flat or LREE-enriched). This REE fractionation signature would be eliminated if all material in the upper mantle were subject to melting as it rose through the 410. Second, conversely, melting in the transition zone in the presence of garnet would yield strongly LREE-enriched liquids. Ascent of such melts would transfer an LREE signature to the upper mantle, yet the most abundant melts derived from the upper mantle (MORB) are observed to be LREE-depleted. Descent of such melts, on the other hand, would allow ascent of residues with low incompatible element contents, yielding a very infertile upper mantle for which there is little evidence. Taken together, these problems suggest that no significant degree of melting occurs near 410 km.

Additional evidence for volatile transport into the lower mantle comes from the study of kimberlite diamond inclusions whose major element compositions strongly suggest a subducted basaltic protolith equilibrated at 700–1400 km depth, as carbon isotopic signatures of the host diamonds are consistent with surface-derived (rather than mantle-derived) carbon (Walter et al., 2011). This adds a pathway to the cycling of material from the surface through the mantle and back again inferred by Hofmann and White (1982) and Eiler et al. (2000).

3.2.3.3 Plume Origins

While much attention has been focused upon the seismological properties of subduction zones, in part because of their significant spatial extent and associated mass flux, seismological studies of hotspot areas are also illuminating, particularly with regard to ascertaining the depth of origin of plume structures. There are two primary types of seismic evidence for constraining the depth of origin of mantle plumes. The first of these consists of seismic tomographic imaging, in which one might expect the achievement of sufficiently fine spatial resolution for imaging narrow plume conduits to be a significant challenge. Indeed, this challenge is further aggravated by the fact that the resolution of such methods tends to decay within the crucial region of the mantle transition zone, which is precisely where one would most like to image a plume in order to determine whether it originated in the shallow or deep mantle.

Nevertheless, seismic tomography has been employed in efforts to image the roots of mantle plumes (VanDecar et al., 1995) and to determine whether or not they arise from deep-seated sources. An instructive example is the case of the Iceland hotspot, which tomographic images suggest may be connected to a deep-seated plume source (Wolfe et al., 1997). Such a conclusion is consistent with the fact that low seismic velocity anomalies appear to extend downward into the transition zone beneath the hotspot, but they do not extend below 150 km beneath the rest of the mid-Atlantic ridge (Montagner and Ritsema, 2001), an observation supported by both global and regional tomography (Allen et al., 2002; Ritsema et al., 1999). However, this interpretation has been challenged. One study (Foulger et al., 2001), claiming tomographic resolution to 450 km depth, concludes that the shape of the imaged low-velocity anomaly changes from cylindrical to tabular near the top of the transition zone, and the investigators argue on the basis of this apparent change in morphology that the plume does not extend to deeper levels. On the other hand, another study (Allen et al., 2002) claiming resolution to 400 km depth reports a simple cylindrical morphology at depth. Detailed numerical tests of the spatial resolution of tomographic imaging under Iceland (Keller et al., 2000) suggest that a deep-seated plume may not be required to explain the observed seismic delay times. In a similar vein, another study (Christiansen et al., 2002) argues that there is a dearth of convincing seismic evidence for a plume extending to depths below 240 km beneath the Yellowstone hotspot, with more recent seismic imaging (James et al., 2011) suggesting a subduction-related origin. All of this serves to highlight some of the persistent ambiguities present in the interpretation of seismic tomographic images beneath hotspots, images which remain nonunique results of the application of a variety of optimization functions to different observational datasets.

The second type of seismic evidence used to constrain the depth of origin of mantle plumes consists of analyses of boundary-interaction phases. Such phases consist of seismic

waves, which, by interacting with the boundaries generally known as seismic 'discontinuities,' have undergone conversion (repartitioning of energy between longitudinal (P) and transverse (S) waves) and/or reflection (repartitioning of energy between upgoing and downgoing waves). For the purposes of studying mantle plumes, the crucial measurements are differential travel times between those phases which interact with the 410 discontinuity and those which interact with the 660 discontinuity. Such differential times translate (via a reference velocity model) into measures of the thickness (depth extent) of the transition zone lying between these two discontinuities.

Given the opposing signs of the Clapeyron slopes of the primary phase transitions associated with these seismic discontinuities, any elevated mantle temperatures associated with thermal plumes may be expected to yield thinning of the transition zone (**Figure 4**), via depression of the 410 and uplift of 660 (Bina, 1998b; Lebedev et al., 2002; Shen et al., 1998). Early global and broad regional studies (Chevrot et al., 1999; Vinnik et al., 1997) failed to detect a clear correlation between such estimates of transition zone thickness and locations of hotspots (Keller et al., 2000), but more recent studies (Courtier et al., 2007) have found such a correlation. Moreover, a number of more localized studies have measured transition zone thinning of several tens of kilometers, suggesting hot thermal anomalies of a few hundred degrees, over regions with diameters of hundreds of kilometers beneath such presumed thermal plume features as the Snake River plain (Dueker and Sheehan, 1997), Iceland (Shen et al., 1998), Yellowstone (Humphreys et al., 2000), Hawaii (Li et al., 2000), and the Society hotspot (Niu et al., 2002). By contrast, no apparent thinning has been found beneath tectonically inactive areas such as the northern North Sea (Helffrich et al., 2003). A straightforward interpretation of these results is that the transition zone beneath plumes is hotter than 'normal' mantle, with thermal plumes originating either deep in the lower mantle below the transition zone or (at the shallowest) in a hot thermal boundary layer at the base of the transition zone.

The picture grows less simple, however, if one attempts to inquire into how the causes of this transition zone thinning are distributed between 410 and 660. Such inquiry involves estimating the actual absolute depths of these two seismic discontinuities beneath plumes. While the use of differential times to estimate thickness requires a reference velocity model within the transition zone, the use of absolute times to estimate individual depths further requires a (laterally varying) reference velocity model from the transition zone to the surface. A simple model of a deep-seated thermal plume suggests that one should observe a depressed 410 with an uplifted 660, which is what seems to be imaged beneath Iceland (Shen et al., 1998). However, one can also find a flat 410 with an uplifted 660 beneath Hawaii (Li et al., 2000), a weakly uplifted 410 with a strongly uplifted 660 beneath the Snake River plain (Dueker and Sheehan, 1997) and Yellowstone (Christiansen et al., 2002; Humphreys et al., 2000), or a depressed 410 with a flat 660 beneath the Society hotspot (Niu et al., 2002). Taken at face value, a depressed (hot) 410 with an uplifted (hot) 660 suggests a plume origin in the lower mantle (Shen et al., 1998). A flat (normal) 410 with an uplifted (hot) 660 suggests either an origin in the lower mantle (Li et al., 2000) or the presence of a thermal boundary layer within the transition zone, as does an uplifted (cold) 410 with uplifted (hot) 660. A depressed (hot) 410 with a flat (normal) 660 suggests an origin within the transition zone (Shen et al., 1998). Interestingly, the one combination which would strongly suggest an origin within the shallow upper mantle, a depressed (hot) 410 with a depressed (cold) 660, is not observed. It is complexities such as these that have led several investigators to argue against the idea of deep-seated plumes in favor of the dominance of upper mantle processes in the origins of hotspots (Anderson, 1994, 2001; Christiansen et al., 2002; Saltzer and Humphreys, 1997), including such detailed proposals as "propagating convective rolls organized by the sense of shear across the aesthenosphere" (Humphreys et al., 2000). This latter proposal would explain a cold 410 overlying a hot 660 (and underlying another hot region near 200 km depth), for example, through localized convection at depths shallower than 400 km (Humphreys et al., 2000).

There are a range of other possible explanations for these seeming complexities, however, a primary factor being the aforementioned reliance of absolute depth estimates for seismic discontinuities upon accurate models of shallow-velocity structures (Helffrich, 2000; Niu et al., 2002; Walck, 1984). If absolute depth estimates are so sensitive to assumptions about shallower structures, then these various and seemingly paradoxical combinations of apparent deflections may arise simply from inaccurate representations of structure outside of the regions of study. Conclusions drawn from differential times, which are free of such dependence upon assumptions about distal regions, may be judged more robust. Such a stance also renders more tractable an understanding of the magnitudes of the implied thermal anomalies. If all of the observed thinning of the transition zone were caused by deflection of either the 410 or 660 alone, then hot temperature anomalies of about 400 K would be required, but the size of the requirement falls to about 200 K if the thinning is shared between anticorrelated 410 and 660 deflections (Helffrich, 2000; Niu et al., 2002).

Another factor to consider is an inherent seismological bias toward underestimating topography. For example, the 'Fresnel zones' that describe the region of the discontinuities that are sampled by boundary-interaction phases can be both large in extent and irregular in shape (Helffrich, 2000; Niu et al., 2002), so that the measured travel times incorporate entwined interactions with both deflected and undeflected portions of a given discontinuity. Moreover, such seismological biases can yield greater underestimates of topography at 410 than at 660 (Helffrich, 2000; Neele et al., 1997), which is consistent with the apparent 'cold 410' puzzle noted earlier. Indeed, some topography simply may not be clearly visible. While the $\alpha \rightarrow \alpha + \beta \rightarrow \beta$ transition should grow sharper at high temperatures as well as being depressed, any small-scale topography on or 'roughening' of discontinuity surfaces can render undetectable the very P-to-S conversions which indicate the presence of topography (Helffrich et al., 2003; van der Lee et al., 1994). Again, such effects may be more significant near 410, where the magnitudes of Clapeyron slopes and hence of topography may be larger (Bina and Helffrich, 1994), but they may also be significant near 660 (van der Lee et al., 1994). Furthermore, the apparent magnitude of discontinuity topography will vary with the frequency of the seismic waves used to probe it (Helffrich, 2000).

The primary point of this discussion, then, is that estimates of lateral variations in transition zone thicknesses from differential seismic travel times are more robust than estimates of lateral variations in the absolute depths of discontinuities from absolute travel times. There are many factors, largely unrelated to plumes, that may cause some underestimation of the former but which induce serious complications in the latter. Certainly, it is possible that the overall tectonic system, including some hotspot-designated volcanic chains, may be controlled to a significant extent from above via the lithosphere rather than from below via the deep mantle (Anderson, 2001). However, the simplest interpretations consistent with observations of transition zone thinning, despite some apparent inconsistencies in estimates of absolute depths of discontinuities, suggest that some hotspots are associated with plume-like thermal anomalies that penetrate the transition zone. Given the great disparities in heat and mass flux among different hotspots, however, there is certainly room for diversity in the family of thermal plumes, and it would not be surprising ultimately to discover various classes of plumes associated with different depths of origin (Kerr, 2003). Aspects of the ongoing debate are summarized, for example, by Campbell and Kerr (2007), Koppers (2011), and associated papers.

3.2.4 Lower Mantle Bulk Composition

3.2.4.1 Bulk Fitting

Given that the properties of the 660 km seismic discontinuity are in excellent agreement with the predicted behavior of an isochemical phase transformation, it might seem reasonable to assume that the lower mantle below this depth possesses largely the same bulk composition as the upper mantle above. This assumption has been regularly challenged, however, based largely upon cosmochemical concerns (Anderson, 1989; Bina, 1998a), upon estimates of mass fluxes between geochemical reservoirs (Helffrich and Wood, 2001), or upon driving forces for chemical differentiation across phase transitions (Bina and Kumazawa, 1993; Garlick, 1969; Kumazawa et al., 1974; Liu and Ågren, 1995; Walker and Agee, 1989). Concern has focused primarily upon whether the lower mantle might be enriched in Fe and/or Si relative to the upper mantle.

One simple way to address this question is to compute profiles of density and bulk sound velocity (thereby avoiding the large uncertainties associated with extrapolating shear moduli), along plausible lower mantle adiabats, for a variety of candidate lower mantle compositions and to compare these model profiles to a reference seismological model such as *ak135* (Kennett et al., 1995). Examination of the root mean square (RMS) misfit between such models over the entire lower mantle quickly reveals several important principles. Density (**Figure 7**) is primarily sensitive to Mg/(Mg+Fe) but not to silica content. Velocity (**Figure 7**) sensitivity, on the other hand, exhibits a trade-off between Mg/(Mg+Fe) and Si/(Mg+Fe). This suborthogonal nature of density and velocity sensitivities allows the two together (**Figures 7** and **8**) to constrain lower mantle composition via the intersection of their respective misfit minima. The resulting family of allowable lower mantle bulk compositions (**Figure 8**) includes a pyrolite mantle composition. While some uncertainty in Si content remains, there is no evidence for bulk Fe enrichment of the lower mantle (**Figure 8**). The extent to which Si enrichment of the lower mantle can be accommodated by the seismological constraints increases as the assumed temperature (at the root of the adiabat) of the lower mantle is increased (**Figure 9**). These schematic results are for a simple lower mantle mineralogy limited to ferromagnesian silicate perovskite (Fiquet et al., 2000), magnesiowüstite (Fei et al., 1992), and stishovite (Li et al., 1996; Liu et al., 1996). Effects of other components (e.g., Ca, Al, Na) have been neglected, and a depth-varying Mg–Fe partitioning coefficient between perovskite and magnesiowüstite (Mao et al., 1997) has been employed. However, repetition of these analyses with the inclusion of Ca-silicate perovskite (Wang et al., 1996) or the use of a depth-invariant partitioning coefficient (Kesson et al., 1998) results in only very minor perturbations, and more sophisticated models (Mattern et al., 2005) yield similar results.

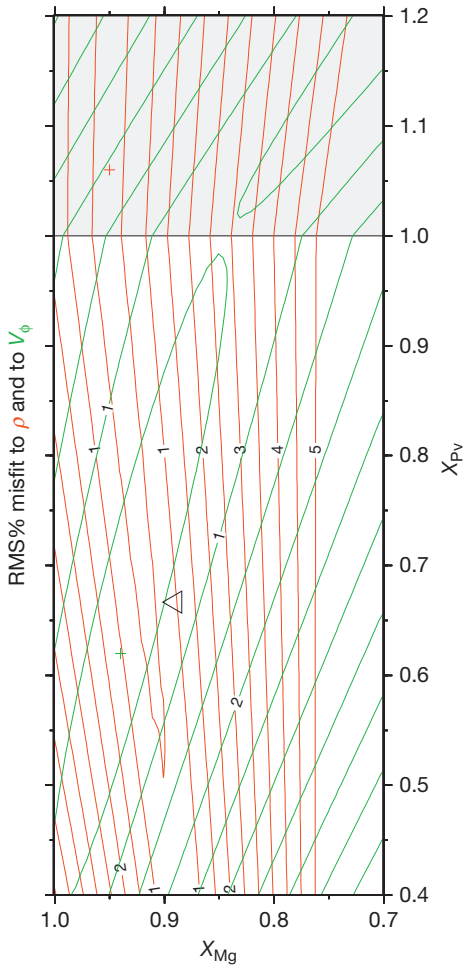

Figure 7 Contours of RMS misfit (%) to seismological reference model *ak135* of density (red) and bulk sound velocity (green) for candidate lower mantle compositions, parameterized in terms of Mg/(Mg+Fe) ($=X_{Mg}$) and Si/(Mg+Fe) ($=X_{Pv}$), over the entirety of the lower mantle. Shaded region at $X_{Pv} > 1$ indicates free silica. Triangle denotes pyrolite. Plus signs denote minima of RMS misfit. Root of lower mantle adiabat is 2000 K at 660 km depth.

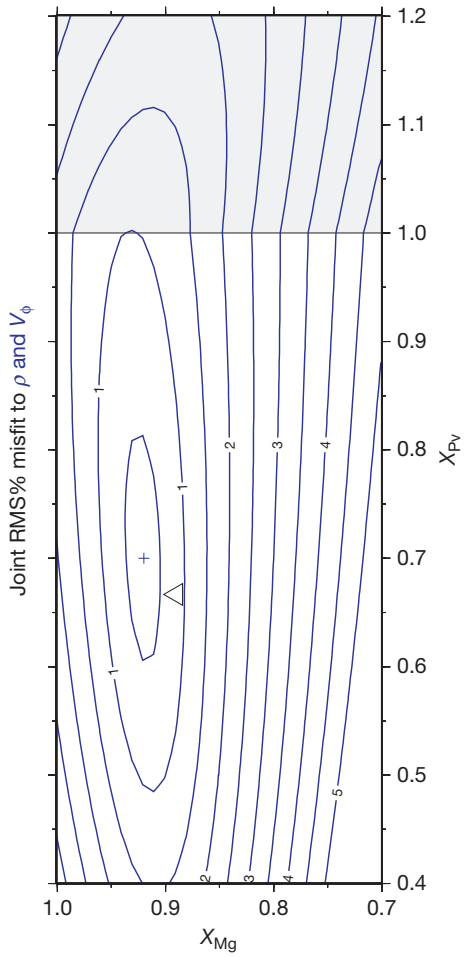

Figure 8 Contours of joint (blue) RMS misfit (%) to seismological reference model *ak135* of density and bulk sound velocity for candidate lower mantle compositions, parameterized in terms of Mg/(Mg + Fe) (=X_{Mg}) and Si/(Mg + Fe) (=X_{Pv}), over the entirety of the lower mantle. Shaded region at $X_{Pv} > 1$ indicates free silica. Triangle denotes pyrolite. Plus sign denotes minimum of RMS misfit. Root of lower mantle adiabat is 2000 K at 660 km depth.

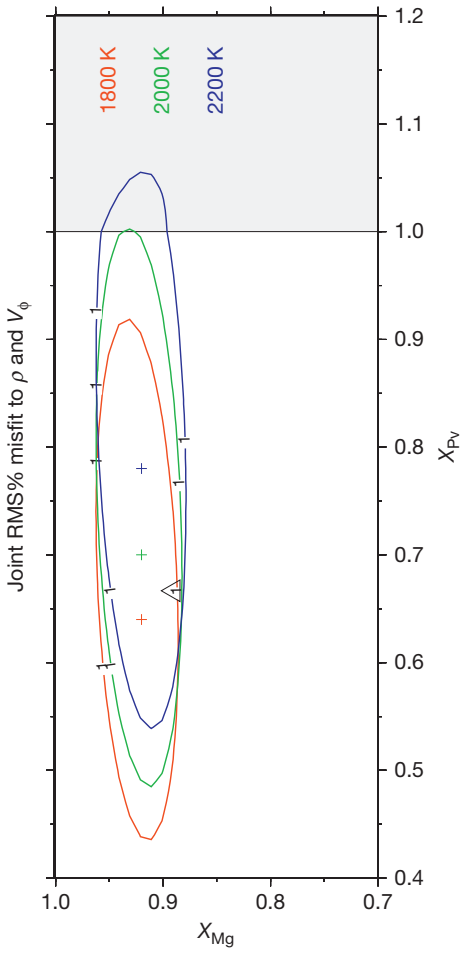

Figure 9 Contours of joint RMS misfit (1%) to seismological reference model *ak135* of density and bulk sound velocity for candidate lower mantle compositions, parameterized in terms of Mg/(Mg + Fe) (=X_{Mg}) and Si/(Mg + Fe) (=X_{Pv}), over the entirety of the lower mantle. Shaded region at $X_{Pv} > 1$ indicates free silica. Triangle denotes pyrolite. Plus signs denotes minima of RMS misfit. Roots of lower mantle adiabats are 1800 (red), 2000 (green), and 2200 K (blue) at 660 km depth.

3.2.4.2 Density Fitting

Seismology provides few direct constraints on the density of materials. The best are from free oscillations of the Earth excited by large earthquakes. The mass of the Earth and its moment of inertia are integral constraints on density, which, combined with the free oscillation (also called 'normal mode') datasets, provide density profiles for the Earth. The most comprehensive of these is the Preliminary Reference Earth Model (PREM) of Dziewonski and Anderson (1981). It seems a straightforward exercise to fit possible mineralogical models of the mantle and core to match densities at particular depths. However, pointwise uncertainties upon density cannot be specified, and no assessment of fit quality is possible. Rather, uncertainties on density are only available for depth averages over some finite interval (Masters and Gubbins, 2003). The narrower the interval, the greater is the uncertainty. Questions such as "Is the lower mantle density profile compatible with pure perovskite?" are well posed, but those such as "Is the density at 800 km depth compatible with pure perovskite?" are not.

3.2.4.3 Depthwise Fitting

A different way of examining these relationships is to plot the best-fitting lower mantle compositions within 10-km-thick depth slices. Again, it is apparent (Figure 10) that density estimates constrain only Mg/(Mg + Fe) while both density and velocity together are required to constrain Si/(Mg + Fe). Bulk sound velocity alone, as shown by the unstable oscillations in best-fitting compositions (Figure 10), does not effectively constrain either compositional parameter within such small depth slices. Throughout most of the lower mantle, there is no evidence for bulk Fe enrichment, and the deviation from a pyrolite composition, in terms of both Mg/(Mg + Fe) and Si/(Mg + Fe), falls within the overall 1% RMS misfit contour (Figure 9). Indeed, the only statistically significant deviations

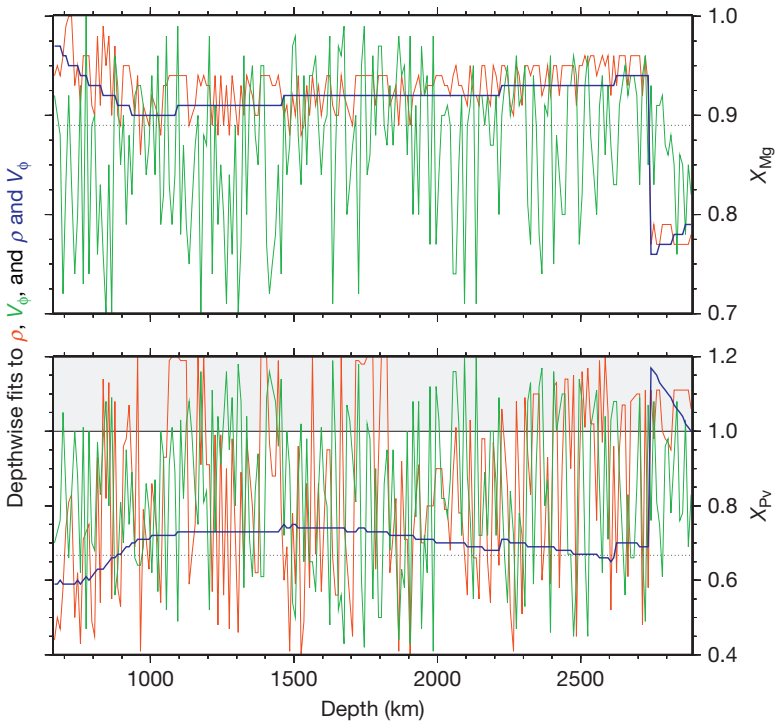

Figure 10 Depthwise best-fit compositions to seismological reference model *ak135* for density alone (red), bulk sound velocity alone (green), and density and bulk sound velocity jointly (blue), with compositions parameterized in terms of Mg/(Mg + Fe) (=X_{Mg}) and Si/(Mg + Fe) (=X_{Pv}), in 10-km-depth slices through the lower mantle. Shaded region at $X_{Pv} > 1$ indicates free silica. Dotted lines (at $X_{Pv} = 0.67$ and $X_{Mg} = 0.89$) denote pyrolite. Root of lower mantle adiabat is 2000 K at 660 km depth.

of the best-fitting composition from pyrolite occur in the top ~300 km of the lower mantle and in the bottom ~200 km. For the former region, this deviation is not surprising, as we probably have not fully incorporated the appropriate mineralogy. While the $\gamma \rightarrow$ pv + mw transition in the olivine component occurs at 660 km depth, the attendant gt → pv transition in the majorite component may not achieve completion until 100 km deeper or more, due to the solubility of Al and ferric Fe in both garnet–majorite and silicate perovskite (McCammon, 1997; Wood and Rubie, 1996). Thus, the anomalous best-fitting compositions in the top 200–300 km of the lower mantle probably arise simply from our omission of garnet from the model mineralogy. The situation in the bottom ~200 km of the lower mantle is more intriguing. Certainly, extrapolations of mineral properties are at their most uncertain in this region, and a globally averaged seismological model such as *ak135* may not accurately reflect details of structure near the core–mantle boundary (CMB). However, it is interesting to note that the implied Fe enrichment and presence of free silica (Figures 10 and 11) are not inconsistent with what one might expect from interactions between silicate lower mantle and metallic core or from accumulation of subducted basaltic material at the CMB. Additional aspects of the CMB region will be addressed further later on. It is interesting to note that recent, more sophisticated efforts to statistically constrain thermal and compositional variations, both radially and laterally throughout the mantle, from seismic tomography models (Deschamps and Trampert, 2003) clearly reiterate four of the basic themes outlined here: silica content is primarily sensitive to velocity, iron content is primarily sensitive to density,

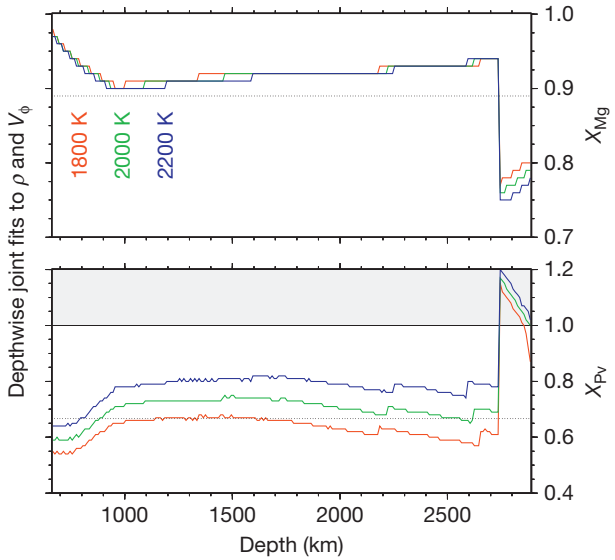

Figure 11 Depthwise best-fit compositions to seismological reference model *ak135* for density and bulk sound velocity jointly, with compositions parameterized in terms of Mg/(Mg + Fe) (X_{Mg}) and Si/(Mg + Fe) (X_{pv}), in 10-km-depth slices through the lower mantle. Shaded region at $X_{Pv} > 1$ indicates free silica. Dotted lines (at $X_{Pv} = 0.67$ and $X_{Mg} = 0.89$) denote pyrolite. Roots of lower mantle adiabats are 1800 (red), 2000 K (green), and 2200 K (blue) at 660 km depth.

compositional (as opposed to thermal) variations are required only in the lowermost part of the mantle, and trade-offs between thermal and compositional effects create non-uniqueness in best-fit models.

Aside from the CMB region, then, a pyrolite lower mantle composition appears to be consistent with seismological constraints. Silica enrichment of the lower mantle can be accommodated if the lower mantle is hotter than expected for a simple adiabat rooted at the 660 km $\gamma \rightarrow \text{pv} + \text{mw}$ transition (**Figure 11**). Because any chemical boundary layer between the upper and lower mantle would be accompanied by a corresponding thermal boundary layer, such a model of a chemically distinct and hot lower mantle is also internally consistent. This trade-off has been evident for decades (Bina and Silver, 1990, 1997; Birch, 1952; Jackson, 1983, 1998; Jeanloz and Knittle, 1989; Mattern et al., 2005; Stixrude et al., 1992; Zhao and Anderson, 1994). However, the seismological evidence (discussed earlier) that the transition zone capping the lower mantle behaves like a set of thermally governed isochemical phase transformations, coupled with the absence of seismic evidence (e.g., a globally sharp seismic reflector displaying hundreds of kilometers of dynamically induced topographic undulations) for a major chemical boundary in the lower mantle, lends considerable support to the minimalist assumption that the bulk composition of the lower mantle greatly resembles that of upper mantle peridotite.

Another aspect of phase relations in the lower mantle, neglected in the preceding simple analysis, is the occurrence of electronic spin transitions at high pressures within the Fe-bearing mantle phases pv and mw (Li et al., 2004; Lin et al., 2010). While such transitions should significantly perturb seismic velocities at very low temperatures, they should be dramatically broadened and damped at the high temperatures of the lower mantle (Cammarano et al., 2010; Lin and Tsuchiya, 2008; Lin et al., 2007; Marquardt et al., 2009). Most analyses to date suggest that such spin transitions should not have a significant impact upon aggregate seismic velocities at lower mantle temperatures, but they do have the potential to significantly affect shear-wave anisotropy (Antonangeli et al., 2011; Cammarano et al., 2010; Crowhurst et al., 2008; Irifune et al., 2010; Marquardt et al., 2009). One exception to this general expectation of only small perturbations in seismic velocities due to spin transitions is a recent study (Mao et al., 2011) reporting that ferromagnesian silicate perovskite, after undergoing high-pressure spin transition, demonstrates an enhanced dependence of bulk modulus upon iron content, possibly allowing for stronger bulk sound velocity depression in response to any local Fe enrichment. There is also some hint of a spin-transition signal in electrical conductivity studies (Velímský, 2010b) and a prediction of significant spin-transition consequences for lower mantle viscosity structure (Matyska et al., 2011).

3.2.5 Lower Mantle Heterogeneity

3.2.5.1 Overview

Seismic velocity heterogeneity in the mantle, as revealed for example by seismic tomography, is often interpreted in terms of strictly thermal origins. However, lateral variations in seismic velocity within the lower mantle (Castle and Creager, 1999; Deuss and Woodhouse, 2002; Hedlin et al., 1997; Niu and Kawakatsu, 1997) may arise from a number of sources, including temperature anomalies (δT), local phase changes (δX_φ), and chemical heterogeneity (δX_i), and they should be accompanied by associated density anomalies. Thus, lower mantle seismic velocity anomalies may reflect local heterogeneity in chemical composition, such as variations in iron/magnesium ratio and silica content, rather than simply variations in temperature. Together, thermal and chemical variations may jointly explain the manner in which the RMS amplitudes of seismic velocity anomalies appear to vary with depth. The distinction is important because velocity anomalies arising from compositional differences are not subject to the same temporal decay as those due to thermal perturbations, due to different timescales for chemical diffusion and thermal conduction.

Temperature anomalies may arise due to low temperatures within cold subducted slab material, but such thermal anomalies will decay with time (and hence depth of penetration into the mantle) as the slab is thermally assimilated into the warmer mantle. Local phase changes are unlikely to occur on significant scales below transition zone depths, except perhaps in exotic compositions containing free oxides (Bina, 1998a). Chemical heterogeneity thus seems a reasonable candidate as a source of seismic velocity heterogeneity in the lower mantle, and an obvious source of major-element chemical heterogeneity is subducted slab material that retains the chemical differentiation acquired during its formation at spreading ridges.

3.2.5.2 Subducted Oceanic Crust

Formation of oceanic lithosphere involves chemical differentiation (by partial melting) of mantle lherzolite parent material (**Chapter 3.3**). The complex structure of oceanic lithosphere closely approximates a simple model of a basaltic–gabbroic crustal layer overlying a depleted harzburgite layer, which in turn overlies lherzolitic peridotite mantle material (**Chapter 3.4**). During subduction, these layers undergo phase transformations to denser phase assemblages with increasing depth of penetration into the mantle. The basalt and gabbro components, for example, progressively transform to eclogite in the upper mantle, to garnetite in the transition zone, and to perovskitite in the lower mantle (Hirose et al., 1999; Kesson et al., 1998; Vacher et al., 1998). Upon deep subduction, all of the components of a petrologically layered slab should transform to a lower mantle mineralogy, consisting of some subset of the phases $(\text{Mg,Fe,Al})\text{SiO}_3$ ferromagnesian silicate perovskite, (Fe,Mg)O, magnesiowüstite, CaSiO_3 calcium silicate perovskite, and SiO_2 stishovite, along with minor amounts of Na-bearing and other phases. The seismic velocities and densities of these layers will differ due, for example, to the coupled effects of Si enrichment and Mg depletion of the basaltic melt relative to the parent mantle.

The temperature dependence of bulk sound velocity for slab compositions is expected to fall with increasing depth in the lower mantle, and the magnitudes of thermal anomalies associated with cold slab material will also fall with increasing

depth as slabs thermally assimilate. Thus, it is difficult to generate large velocity anomalies at depth by temperature perturbations alone. On the other hand, the composition dependence of bulk sound velocity is significantly greater. In particular, basaltic crustal compositions yield significantly fast velocity anomalies relative to underlying harzburgite and peridotite layers, and anomaly magnitudes increase with depth. Hence, it should be easier to generate large velocity anomalies through compositional variations, such as those associated with subducted slabs (Bina, 2003; Ricard et al., 2005; Rost et al., 2008).

High velocities in subducted basaltic material should arise largely from the presence of free silica phases, initially in the form of stishovite. At higher pressures, stishovite transforms to a $CaCl_2$-structured phase of SiO_2 and ultimately to α-PbO_2-structured seifertite. Such free silica, however, should react with magnesiowüstite in the surrounding lower mantle material to form silicate perovskite. Thus, survival of free silica in the lower mantle may require formation of perovskite rinds to preserve the free silica from reaction with magnesiowüstite, just as porphyroblasts can protect inclusions (which would otherwise become reactants) to form 'armored relics' in more familiar metamorphic rocks (Bina, 2010).

Damping and smearing arising from regularization in seismic tomography typically cause narrow, intense anomalies to be imaged as broader, more subdued anomalies (Garnero, 2000). Thus, layers of basaltic material ~10 km thick that are ~5% fast, for example, might reasonably be expected to appear as ~0.5% velocity anomalies distributed over 100 km thick slabs. If this is the case, then one might seek frequency-dependent effects in seismological observations, in which the apparent magnitude of velocity anomalies rises with the spatial resolving power of the seismic probe.

Studies of lower mantle seismic scatterers, on the other hand, have suggested that bodies of 10 km or less in size exhibit velocity anomalies of several percent (Garnero, 2000; Hedlin et al., 1997; Kaneshima and Helffrich, 1998, 1999, 2010; Niu et al., 2003), especially near subduction zones. Such narrow velocity anomalies appear to be consistent with an origin in subducted oceanic lithosphere. While some fast anomalies have been reported at relatively shallow depths, consistent with origins in stishovite, many of the scatterers in the 1200–1800 km depth range appear to be seismically slow. Such slow anomalies may reflect the transformation of stishovite to the $CaCl_2$-structured phase of SiO_2 via a displacive transition that results in a depressed shear modulus over a broad pressure range, with shear softening by up to 20% expected (Carpenter et al., 2000; Jiang et al., 2009; Karki et al., 1997; Shieh et al., 2002). The expected depth range of this shear softening in SiO_2 largely coincides with that of the observed slow scatterers, although the shallowest observations seem to require slight shifting of the transition in pure SiO_2 to lower pressures via incorporation of H_2O and Al_2O_3 components (Hirose et al., 2005; Tsuchiya et al., 2004a).

Velocity perturbations arising from thermal and compositional anomalies will be accompanied by associated density anomalies. Former basaltic crustal material should be significantly denser than peridotite (**Figure 12**) under all lower mantle conditions below a depth of 720 km, even if it has fully thermally equilibrated with its surroundings (Bina, 2003; Fukao et al., 2009; Ricolleau et al., 2010). Thus, although the common mapping of fast velocity anomalies into low temperatures appears to be a serious oversimplification, in view of the large potential for compositional sources, the usual mapping of fast anomalies into positive density (i.e., negative buoyancy) anomalies does appear to survive in the presence of chemical differentiation.

The above discussion, of course, assumes that subducted basaltic material is transported through the transition zone into the lower mantle. It has, however, been suggested that density contrasts between basalt and underlying harzburgite and peridotite in the transition zone – especially the postulated attainment of nearly neutral buoyancy by eclogites near 660 km depth – may lead to physical separation by delamination and trapping of eclogite near the base of the transition zone (Hirose et al., 1999; Irifune and Ringwood, 1993; Ringwood and Irifune, 1988). Subsequent studies over a broader range of temperatures (Aoki and Takahashi, 2004), however, suggest that eclogites should be somewhat denser than previously estimated, at least in the upper portion of the transition zone, and studies of hydrous systems (Litasov et al., 2004, 2006) indicate that the basalt–peridotite density crossover in the transition zone does not occur in water-bearing compositions. Moreover, delamination of basalt from a subducting slab depends upon contrasts not only in buoyancy but also in rheology. Geodynamical modeling studies over a range of viscosity structures suggest that any layer of trapped basalt could be only marginally stable (Christensen, 1988) and that a basaltic layer is unlikely to separate (Gaherty and Hager, 1994), although others suggest that separation may be feasible if an anomalously weak layer is present just below the crust (Karato, 1997; Van Keken et al., 1996). Incorporation of kinetics (Ganguly et al., 2009) and more realistic compositions (Nakagawa et al., 2010) into such models, however, further decreases the expected degree of any such basaltic separation and segregation.

Indeed, the successful transport of basaltic crustal material into the lower mantle is also suggested by the observation of small seismic scatterers in the lower mantle (Kaneshima and Helffrich, 2009) and their likely origin in the high-pressure silica phases expected to form under such conditions (Bina, 2010). The applicability of the mechanical mixture model (Xu et al., 2008) to the lower mantle also depends upon deep subduction of basalts. If the scattering objects observed in the lower mantle actually are subducted crust, their maximum scale length precludes formation of a large mélange of metabasalt and harzburgite – the 'megalith' of Ringwood and Irifune (1988) – with scale lengths in excess of 100 km. No scatterer larger than about 10 km has been found (Kaneshima and Helffrich, 2009). Scatterer arrays appear in large-scale sheetlike structures and change their visibility when illuminated with different polarizations of shear-wave energy (Kaneshima and Helffrich, 1998, 2009). These are features expected for wholesale subduction of crustal material into the lower mantle rather than segregation atop the lower mantle. Further evidence of successful transport of basaltic crust into the lower mantle is found in kimberlite diamond inclusions whose major element compositions suggest subducted basalt equilibrated at 700–1400 km depth (Walter et al., 2011).

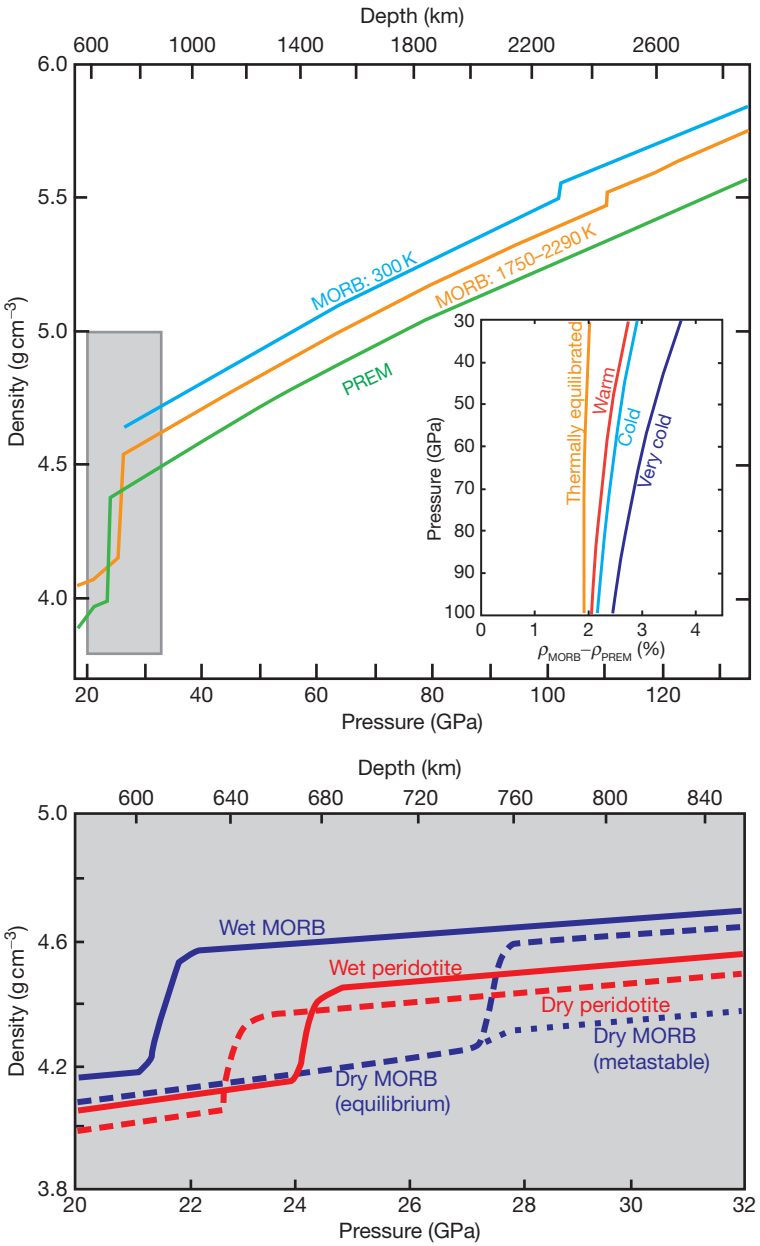

Figure 12 Density differences (top) between cold (blue) and warm (orange) MORB and ambient mantle as represented by PREM (green) (modified from figure 16 of Fukao et al., 2009). Gray box indicates depth where MORB might be less dense than peridotite. Density contrasts (inset) between MORB and PREM along various slab geotherms (modified from figure 7 of Ricolleau et al., 2010) decrease at the base of the mantle, but MORB always remains denser. The density inversion (bottom) observed in dry compositions does not occur in wet or metastable systems (modified from figure 6 of Ohtani and Litasov, 2006).

3.2.5.3 Heterogeneity Profiles with Depth

The first evidence for different structures of seismic heterogeneity in the mantle arose from the use of global datasets. Both Su and Dziewonski (1991) and Woodward and Masters (1991) showed structural differences in deep mantle anomalies as compared to shallow mantle anomalies. The power in the spectral coefficients of Su and Dziewonski's (1991) study was concentrated at degrees corresponding to 6000 km laterally, and power was extremely low below depths of 1500 km. Woodward and Masters (1991) showed that lower mantle heterogeneity rose again at the base of the mantle, attaining twice the heterogeneity near the CMB compared to mid–lower mantle levels. This established the view that the lower mantle was more homogeneous than the upper mantle or CMB for long-period body waves.

At shorter periods, the picture of lower mantle heterogeneity differs. Systematic studies of scattered waves in the lower mantle around the Pacific Ocean basin detect scattered energy of uniform intensity from the top of the lower mantle down to approximately 1600 km depth (Kaneshima and Helffrich,

2009). Below this level, scattered energy decreases. Thus, there is significant small-scale heterogeneity in the lower mantle, but it is distributed more homogeneously in depth until it fades in the deep lower mantle. Whether it recurs at the CMB is an open question that requires different study methods (Ivan and Cormier, 2011; Thomas et al., 2009).

3.2.5.4 Lowermost Mantle

The lowermost D″ layer of the mantle exhibits a number of unusual geophysical features suggestive of possible compositional complexities. These include observations of multiple seismic discontinuities overlying negative velocity gradients, ultralow-velocity zones (ULVZs), anticorrelated lateral variations in V_S and V_φ, and large low-shear-velocity provinces (LLSVPs) extending from the CMB through D″ hundreds of kilometers upward. Interpretations of such features have focused upon possible radial and lateral variations in both temperature and chemical composition, possible zones of partial melting, and potential roles of the post-perovskite phase transition.

Most earlier attempts to estimate variations in V_φ or ρ from seismic tomography results assumed a constant $d\ln\rho/d\ln V_S$ scaling, because the body-wave travel times upon which they were based were fundamentally insensitive to density variations. More recently, however, seismic data from the Earth's normal modes of free oscillation, which are sensitive to density over broad depth ranges, have allowed the removal of such artificial scaling constraints (Ishii and Tromp, 1999, 2004), a welcome development given the apparent divergence from velocity–density scaling systematics for shear-wave speeds (Zaug et al., 1993). Such studies have revealed regions at the base of the lower mantle which exhibit anomalies characterized by low V_S, high V_φ, and high ρ. As it is difficult to obtain such anticorrelated variations in V_S and V_φ (or ρ) through thermal perturbations alone (unless such thermal perturbations happen to occur near a phase-transition boundary, such as pv→ppv discussed later), such observations are generally interpreted as evidence for lateral heterogeneity in chemical composition. Statistical analysis of the fitting of long-period seismic data (Resovsky and Trampert, 2003) indicates that such anticorrelations are robust to damping effects. Statistical inversions of tomographic models for compositional perturbations (Deschamps and Trampert, 2003) suggest variations in silicate content of order 10% and in iron content of order 1% in the lowermost mantle, while analyses based on body-wave travel times combined with various geodynamic constraints suggest somewhat smaller compositional variations (Simmons et al., 2010).

Analysis of seismic phases interacting with ULVZs (Garnero and Helmberger, 1996; Lay et al., 1998; Thorne and Garnero, 2004; Zhang et al., 2009) suggests that these regions typically exhibit V_S reduction by 20–30% over a depth range of 10–20 km. Such properties are commonly inferred to indicate the presence of partial melt (with melt fraction of order 10%) just above the CMB (Fiquet et al., 2010; Stixrude et al., 2009). Uncertainties in lower mantle rheological properties certainly allow for the geotherm to exceed the solidus (Matyska and Yuen, 2007), and it has been argued that dynamic pressure gradients may be sufficient to stabilize such a melt layer (Hernlund and Jellinek, 2010). However, recent measurements also suggest that ULVZ signatures could arise from chemically distinct zones (of mantle peridotite with 10–20% Fe-enriched mw) in the complete absence of melting (Bower et al., 2011; Wicks et al., 2010).

In addition to global mapping of ULVZs, such mapping has also been undertaken of the so-called D″ discontinuities (Lay et al., 1998). Originally perceived as a single seismic discontinuity at 100–350 km above the CMB overlying a slightly negative vertical gradient in velocity, these features have more recently been imaged as a pair of discontinuities or even as a quadruplet of stacked discontinuities. Discovery of the transition of ferromagnesian silicate perovskite (pv) to the so-called post-perovskite (ppv) phase (Murakami et al., 2004; Oganov and Ono, 2004; Tsuchiya et al., 2004b) has led to efforts to interpret such discontinuities in the framework of this phase transition. Rather than simply transforming to ppv around 100–300 km above the CMB, it is envisioned that the positive dP/dT slope of the transition, combined with a steep temperature gradient in the thermal boundary layer above the CMB, may allow two successive intersections with the phase boundary, pv→ppv→pv, at least for colder geotherms (Hirose and Lay, 2008; Lay et al., 2006; Wookey et al., 2005) – a 'double-crossing' analogous to the spinel→plagioclase→spinel lherzolite succession of transitions in warm lithosphere (Kaus et al., 2005; Wood and Yuen, 1983). Furthermore, the depth and width of the pv→ppv transition will vary with composition, shifting to lower pressure and broadening in depth extent in compositions with basaltic Al content (Tsuchiya and Tsuchiya, 2008) and Fe/Mg ratio, while simultaneously coinciding with the transition from $CaCl_2$-structured SiO_2 to α-PbO_2-structured seifertite in basalt (Ohta et al., 2008). The combined effects of lateral variations in thermal gradient and chemical composition upon multiple ppv transitions in a mechanical mixture of peridotite and basalt, followed by the onset of partial melting, have been invoked in an attempt to explain observations of quadruple D″ discontinuities (Ohta et al., 2008). The intersections of plausible geotherms (Hirose and Lay, 2008; Katsura et al., 2010; Wookey et al., 2005) with phase boundaries in multicomponent systems (**Figure 13**) suggest that multiple crossings are unlikely except when lateral temperature variations arise near the CMB (and possibly no crossings at all given phase boundary uncertainty).

Upon simultaneous consideration of such seismological observations as ULVZs, LLSVPs, and D″ discontinuities, it seems that low-V_S regions in the lowermost mantle may arise either from lateral variations in chemical composition or from ppv lenses, whose extent is controlled by lateral variations in temperature gradient (Hernlund and Houser, 2008). Thus, current sketches of CMB structure (**Figure 14**) generally simultaneously include lateral variations in composition (from peridotite to basalt), large temperature gradients, regions of stability of post-perovskite, and some extent of partial melting (Hirose and Lay, 2008). Enhanced levels of seismic anisotropy in the D″ region, the analysis of which lies beyond the scope of this review, have also been interpreted in the post-perovskite framework, in terms of stacking faults within the ppv phase (Oganov et al., 2005).

Further complexities are introduced by the observation of auto-redox reactions ($3Fe^{2+}O \rightarrow Fe^0 + Fe^{3+}{}_2O_3$) in

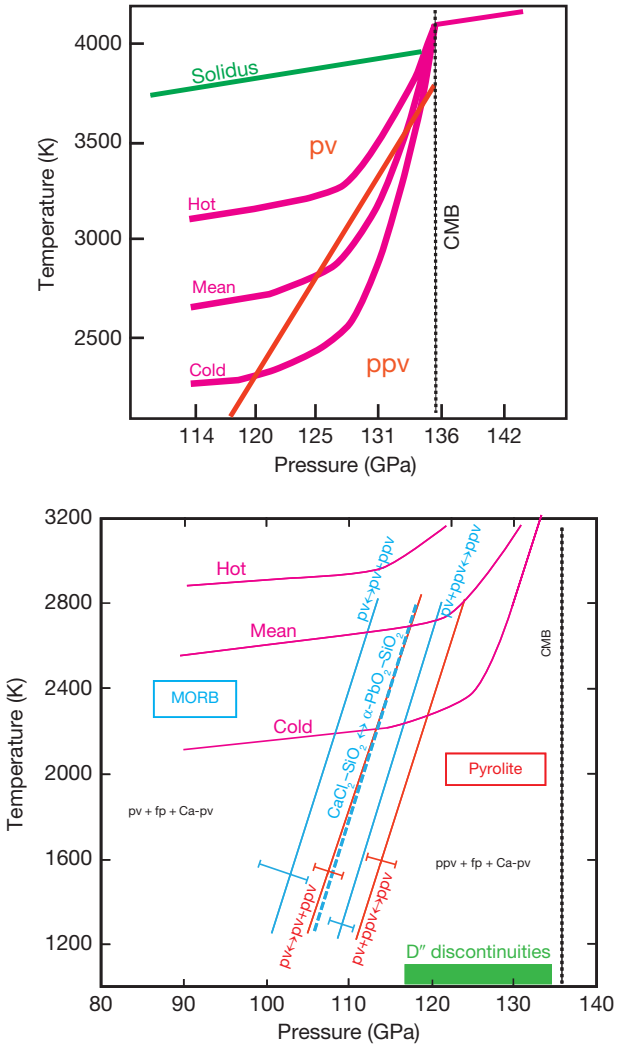

Figure 13 Schematic model (top) of possible origin of pair of D″ discontinuities in double crossing of pv↔ppv transition for certain cooler geotherms (modified from figure 5 of Hirose and Lay, 2008). The phase boundaries near the CMB (dotted) potentially cross the pv↔ppv boundary (red), leading to no or two seismic discontinuities. Phase boundaries (bottom) with error bars, exhibiting mixed-phase regions in multicomponent systems for pyrolite (red) and basalt (blue) (modified from figures 4 and 5 of Ohta et al., 2008), overlain with model geotherms (mauve) of Hirose and Lay (2008) extended to lower pressures using adiabatic gradient of Katsura et al. (2010). Green bar shows range of observed D″ discontinuities. Note shift of phase boundaries to lower pressures for MORB compositions (which also exhibit a phase change in free silica shown by the dashed blue line). Two pairs of D″ discontinuities might arise in regions of compositional heterogeneity within uncertainties for more strongly curved geotherms, such as those of Wookey et al. (2005).

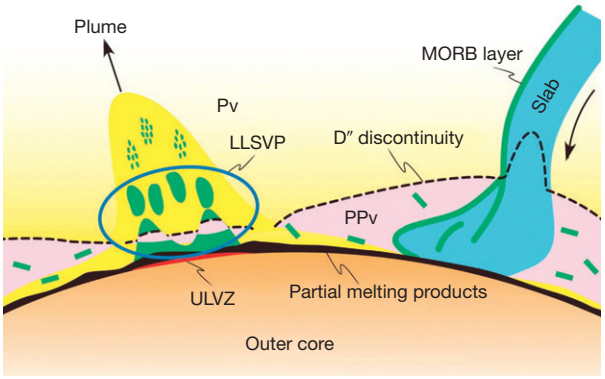

Figure 14 A summary cartoon of the CMB region, showing D″ seismic discontinuities associated with pv↔ppv transitions, their depth variation due to lateral changes in temperature and composition (mantle peridotite vs. subducted MORB), partial melting zones, ultralow velocity zones (ULVZs), and large low-shear-velocity provinces (LLSVPs), together with possible plume-source associations. Reproduced from Hirose K and Lay T (2008) Discovery of post-perovskite and new views on the core-mantle boundary region. *Elements* 4: 183–189, figure 6, with permission from the Mineralogical Society of America.

ferro-magnesian silicate perovskite under deep lower mantle conditions, yielding small amounts of iron metal (Frost et al., 2004). While theory suggests that such auto-redox may occur in both pv and ppv (Zhang and Oganov, 2006), recent experiments suggest that it occurs only in pv. If true, then transition to ppv should partition Fe into fp, thereby depleting ppv in Fe and sharpening the pv→ppv transition (Sinmyo et al., 2011) – somewhat analogous to the sharpening of the $\alpha \rightarrow \beta$ transition due to Fe–Mg exchange between olivine and garnet in the upper mantle (Irifune and Isshiki, 1998). Furthermore, a recent report of metallization of FeO under lowermost mantle conditions, in connection with an electronic spin transition but without any apparent structural phase transition, suggests the possibility of exsolution in ferropericlase, thus further complicating phase relations in this region (Ohta et al., 2012).

3.2.6 Future Prospects

In science, future predictions are a mug's game because so many new research directions arise serendipitously. Most attempts, including this one, document the predictor's frustration at seeing unfinished work rendered uninteresting by new developments. Of the issues related to this review, the top question is whether post-perovskite is a reality on the Earth. Remaining uncertainties in laboratory pressure scales, CMB temperatures, and reaction compositional dependences allow for the possibility that the ppv phase may never attain stability in the terrestrial lower mantle. Resolving this question would significantly clarify the debate on the phenomena at the bottom of the Earth's mantle. Another issue arising in this area is whether there is any role for melting in the development of seismic structures at the CMB. Seismic properties, particularly those of shear waves and anisotropy, are very sensitive to small melt amounts. Systematic study of their properties would enlighten the discipline. In a similar vein, better CMB temperature constraints might be gained from improved material-property knowledge of both mantle and core materials. The discovery of layering in the outer core could potentially be used to sharpen core-side constraints. Furthermore, the apparent seismological detection of long-elusive metastable olivine in subduction zones calls for reconciliation with laboratory

studies of transformation kinetics, potentially illuminating hydration–dehydration processes. Finally, development of systematic methods to globally find seismic scatterers and assess their spatial concentration should help to close the gap between geochemical signals and the physical processes that generate them.

Acknowledgments

CRB is grateful to the Department of Geophysics, Charles University, Prague, where portions of this writing were performed while a visiting researcher. We thank Tom Duffy for a helpful review and Rick Carlson for both critical comments and immense editorial patience.

References

Agee CB (1998) Phase transformations and seismic structure in the upper mantle and transition zone. *Reviews in Mineralogy* 37: 165–203.

Ai Y, Zheng T, Xu W, He Y, and Dong D (2003) A complex 660 km discontinuity beneath northeast China. *Earth and Planetary Science Letters* 212: 63–71.

Allen RM, Nolet G, Morgan WJ, et al. (2002) Imaging the mantle beneath Iceland using integrated seismological techniques. *Journal of Geophysical Research* 107(B12): 23–25.

Anderson DL (1979) The upper mantle transition region: Eclogite? *Geophysical Research Letters* 6: 433–436.

Anderson DL (1982) Chemical composition and evolution of the mantle. In: Akimoto S and Manghnani MH (eds.) *High Pressure Research in Geophysics*, pp. 301–318. Tokyo: Center for Academic Publication.

Anderson DL (1984) The earth as a planet: Paradigms and paradoxes. *Science* 223: 347–355.

Anderson DL (1989) Composition of the Earth. *Science* 243: 367–370.

Anderson DL (1994) The sublithospheric mantle as the source of continental flood basalts: The case against the continental lithosphere and plume head reservoirs. *Earth and Planetary Science Letters* 123: 269–280.

Anderson DL (2001) Top-down tectonics? *Science* 293: 2016–2018.

Anderson DL and Bass JD (1984) Mineralogy and composition of the upper mantle. *Geophysical Research Letters* 11: 637–640.

Anderson DL and Bass JD (1986) Transition region of the Earth's upper mantle. *Nature* 320: 321–328.

Andrews J and Deuss A (2008) Detailed nature of the 660 km region of the mantle from global receiver function data. *Journal of Geophysical Research* 113: B06304.

Antonangeli D, Siebert J, Aracne CM, et al. (2011) Spin crossover in ferropericlase at high pressure: A seismologically transparent transition? *Science* 331: 64–67.

Aoki I and Takahashi E (2004) Density of MORB eclogite in the upper mantle. *Physics of the Earth and Planetary Interiors* 143–144: 129–143.

Bass JD and Anderson DL (1984) Composition of the upper mantle: Geophysical tests of two petrological models. *Geophysical Research Letters* 11: 229–232.

Bercovici D and Karato SI (2003) Whole mantle convection and the transition-zone water filter. *Nature* 425: 39–44.

Bianchini G, Beccaluva L, Bonadiman C, Nowell GM, Pearson DG, and Wilson M (2010) Mantle metasomatism by melts of HIMU piclogite components: New insights from Fe-lherzolite xenoliths (Calatrava Volcanic District, central Spain). In: Coltorti M, Downes H, Gregoire M, and O'Reilly SY (eds.) *Petrological Evolution of the European Lithospheric Mantle*, *Geological Society Special Publication* 337, pp. 107–124. London: Geological Society of London.

Bina CR (1998a) Lower mantle mineralogy and the geophysical perspective. *Reviews in Mineralogy* 37: 205–239.

Bina CR (1998b) Free energy minimization by simulated annealing with applications to lithospheric slabs and mantle plumes. *Pure and Applied Geophysics* 151: 605–618.

Bina CR (2003) Seismological constraints upon mantle composition. In: Carlson RW (ed.) *Treatise on Geochemistry, Vol 2: The Mantle and Core*, pp. 39–59. Oxford: Elsevier.

Bina CR (2010) Scale limits of free-silica seismic scatterers in the lower mantle. *Physics of the Earth and Planetary Interiors* 183: 110–114.

Bina CR and Helffrich GR (1992) Calculation of elastic properties from thermodynamic equation of state principles. *Annual Review of Earth and Planetary Sciences* 20: 527–552.

Bina CR and Helffrich G (1994) Phase transition Clapeyron slopes and transition zone seismic discontinuity topography. *Journal of Geophysical Research* 99: 15853–15860.

Bina CR and Kumazawa M (1993) Thermodynamic coupling of phase and chemical boundaries in planetary interiors. *Physics of the Earth and Planetary Interiors* 76: 329–341.

Bina CR and Silver PG (1990) Constraints on lower mantle composition and temperature from density and bulk sound velocity profiles. *Geophysical Research Letters* 17: 1153–1156.

Bina CR and Silver PG (1997) Bulk sound travel times and implications for mantle composition and outer core heterogeneity. *Geophysical Research Letters* 24: 499–502.

Bina CR and Wood BJ (1987) The olivine-spinel transitions: Experimental and thermodynamic constraints and implications for the nature of the 400 km seismic discontinuity. *Journal of Geophysical Research* 92: 4853–4866.

Birch F (1952) Elasticity and constitution of the Earth's interior. *Journal of Geophysical Research* 57: 227–286.

Bower DJ, Wicks JK, Gurnis M, and Jackson JM (2011) A geodynamic and mineral physics model of a solid-state ultralow-velocity zone. *Earth and Planetary Science Letters* 303: 193–202.

Cammarano F, Marquardt H, Speciale S, and Tackley PJ (2010) Role of iron-spin transition in ferropericlase on seismic interpretation: A broad thermochemical transition in the mid mantle? *Geophysical Research Letters* 37: L03308.

Cammarano F and Romanowicz B (2007) Insights into the nature of the transition zone from physically constrained inversion of long-period seismic data. *Proceedings of the National Academy of Sciences of the United States of America* 104: 9139–9144.

Campbell IH and Kerr AC (2007) The great plume debate: Testing the plume theory. *Chemical Geology* 241: 149–152.

Carpenter MA, Hemley RJ, and Mao HK (2000) High-pressure elasticity of stishovite and the P42/mnm to Pnnm phase transition. *Journal of Geophysical Research* 105: 10807–10816.

Castle JC and Creager KC (1999) A steeply dipping discontinuity in the lower mantle beneath Izu-Bonin. *Journal of Geophysical Research* 104: 7279–7292.

Chevrot S, Vinnik L, and Montagner J-P (1999) Global-scale analysis of the mantle Pds phases. *Journal of Geophysical Research* 104: 20203–20220.

Christensen U (1988) Is subducted lithosphere trapped at the 670-km discontinuity? *Nature* 336: 462–463.

Christiansen RL, Foulger GR, and Evans JR (2002) Upper-mantle origin of the yellowstone hotspot. *Geological Society of America Bulletin* 114: 1245–1256.

Connolly JAD and Kerrick DM (2002) Metamorphic controls on seismic velocity of subducted oceanic crust at 100–250 km depth. *Earth and Planetary Science Letters* 204: 61–74.

Courtier AM, Jackson MG, Lawrence JF, et al. (2007) Correlation of seismic and petrologic thermometers suggests deep thermal anomalies beneath hotspots. *Earth and Planetary Science Letters* 264: 308–316.

Crowhurst JC, Brown JM, Goncharov AF, and Jacobsen SD (2008) Elasticity of (Mg, Fe)O through the spin transition of iron in the lower mantle. *Science* 319: 451–453.

Deschamps F and Trampert J (2003) Mantle tomography and its relation to temperature and composition. *Physics of the Earth and Planetary Interiors* 140: 277–291.

Deuss A, Redfern SAT, Chambers K, and Woodhouse JH (2006) The nature of the 660-kilometer discontinuity in Earth's mantle from global seismic observations of PP precursors. *Science* 311: 198–201.

Deuss A and Woodhouse JH (2001) Seismic observations of splitting of the mid-mantle transition zone discontinuity in Earth's mantle. *Science* 294: 354–357.

Deuss A and Woodhouse JH (2002) A systematic search for mantle discontinuities using SS-precursors. *Geophysical Research Letters* 29(8): 1241.

Dueker KG and Sheehan AF (1997) Mantle discontinuity structure from midpoint stacks of converted P and S waves across the Yellowstone hotspot track. *Journal of Geophysical Research* 102: 8313–8328.

Duffy TS and Anderson DL (1989) Seismic velocities in mantle minerals and the mineralogy of the upper mantle. *Journal of Geophysical Research* 94: 1895–1912.

Duffy TS, Zha CS, Downs RT, Mao HK, and Hemley RJ (1995) Elasticity of forsterite to 16 GPa and the composition of the upper mantle. *Nature* 378: 170–173.

Dziewonski AM and Anderson DL (1981) Preliminary reference Earth model. *Physics of the Earth and Planetary Interiors* 25: 297–356.

Eiler JM, Schiano P, Kitchen N, and Stolper EM (2000) Oxygen isotope evidence for recycled crust in the sources of mid-ocean ridge basalts. *Nature* 403: 530–534.

Fei Y, Mao H-K, and Mysen BO (1991) Experimental determination of element partitioning and calculation of phase relations in the MgO-FeO-SiO_2 system at high pressure and high temperature. *Journal of Geophysical Research* 96: 2157–2169.

Fei Y, Mao H-K, Shu J, and Hu J (1992) P-V-T equation of state of magnesiowüstite $(Mg_{0.6}Fe_{0.4})O$. *Physics and Chemistry of Minerals* 18: 416–422.

Fiquet G, Auzenda AL, Siebert J, et al. (2010) Melting of peridotite to 140 gigapascals. *Science* 329: 1516–1518.

Fiquet G, Dewaele A, Andrault D, Kunz M, and LeBihan T (2000) Thermoelastic properties and crystal structure of $MgSiO_3$ perovskite at lower mantle pressure and temperature conditions. *Geophysical Research Letters* 27: 2124.

Flesch LM, Li B, and Liebermann RC (1998) Sound velocities of polycrystalline $MgSiO_3$-orthopyroxene to 10 GPa at room temperature. *American Mineralogist* 83: 444–450.

Foulger GR, Pritchard MJ, Julian BR, et al. (2001) Seismic tomography shows that upwelling beneath Iceland is confined to the upper mantle. *Geophysical Journal International* 146: 504–530.

Frost DJ (2003) The structure and sharpness of $(Mg,Fe)_2SiO_4$ phase transformations in the transition zone. *Earth and Planetary Science Letters* 216: 313–328.

Frost DJ, Liebske C, Langenhorst F, McCammon CA, Trønnes RG, and Rubie DC (2004) Experimental evidence for the existence of iron-rich metal in the Earth's lower mantle. *Nature* 428: 409–412.

Fukao Y, Obayashi M, Nakakuki T, et al. (2009) Stagnant slab: A review. *Annual Review of Earth and Planetary Sciences* 37: 19–46.

Fukao Y, Widiyantoro S, and Obayashi M (2001) Stagnant slabs in the upper and lower mantle transition region. *Reviews of Geophysics* 39: 291–323.

Gaherty JB and Hager BH (1994) Compositional vs. thermal buoyancy and the evolution of subducted lithosphere. *Geophysical Research Letters* 21: 141–144.

Ganguly J, Freed AM, and Saxena SK (2009) Density profiles of oceanic slabs and surrounding mantle: Integrated thermodynamic and thermal modeling, and implications for the fate of slabs at the 660 km discontinuity. *Physics of the Earth and Planetary Interiors* 172: 257–267.

Garlick GD (1969) Consequences of chemical equilibrium across phase changes in the mantle. *Lithos* 2: 325–331.

Garnero EJ (2000) Heterogeneity of the lowermost mantle. *Annual Review of Earth and Planetary Sciences* 28: 509–537.

Garnero EJ and Helmberger DV (1996) Seismic detection of a thin laterally varying boundary layer at the base of the mantle beneath the central-Pacific. *Geophysical Research Letters* 23: 977–980.

Gilbert HJ, Sheehan AF, Dueker KG, and Molnar P (2003) Receiver functions in the western United States, with implications for upper mantle structure and dynamics. *Journal of Geophysical Research* 108(B5): 2229.

Green HW II, Chen W-P, and Brudzinski MR (2010) Seismic evidence of negligible water carried below 400-km depth in subducting lithosphere. *Nature* 476: 828–831.

Green HW II and Houston H (1995) The mechanics of deep earthquakes. *Annual Review of Earth and Planetary Sciences* 23: 169–213.

Gu YJ and Dziewonski AM (2002) Global variability of transition zone thickness. *Journal of Geophysical Research* 107(B7): 2135.

Gu Y, Dziewonski AM, and Agee CB (1998) Global de-correlation of the topography of transition zone discontinuities. *Earth and Planetary Science Letters* 157: 57–67.

Haak V and Hutton VSR (1986) Electrical resistivity in continental lower crust. In: Dawson JB, Carswell DA, Hall J, and Wedepohl KH (eds.) *The Nature of the Lower Continental Crust, Geological Society Special Publication* 24, pp. 35–49. London: Geological Society of London.

Hacker BR (1996) Eclogite formation and the rheology, buoyancy, seismicity, and H2O content of oceanic crust. In: Bebout G, Scholl D, Kirby S, and Platt J (eds.) *Subduction Top to Bottom, Geophysical Monograph Series*, vol. 96, pp. 337–346. Washington, DC: American Geophysical Union.

Hedlin MAH, Shearer PM, and Earle PS (1997) Seismic evidence for small-scale heterogeneity throughout the Earth's mantle. *Nature* 387: 145–150.

Helffrich G (1996) Subducted lithospheric slab velocity structure: Observations and mineralogical inferences. In: Bebout G, Scholl D, Kirby S, and Platt J (eds.) *Subduction Top to Bottom, Geophysical Monograph Series*, vol. 96, pp. 215–222. Washington, DC: American Geophysical Union.

Helffrich G (2000) Topography of the transition zone seismic discontinuities. *Reviews of Geophysics* 38: 141–158.

Helffrich G, Asencio E, Knapp J, and Owens T (2003) Transition zone structure in a tectonically inactive area: 410 and 660 km discontinuity properties under the northern North Sea. *Geophysical Journal International* 155: 193–199.

Helffrich G and Bina CR (1994) Frequency dependence of the visibility and depths of mantle seismic discontinuities. *Geophysical Research Letters* 21: 2613–2616.

Helffrich G and Stein S (1993) Study of the structure of the slab-mantle interface using reflected and converted seismic waves. *Geophysical Journal International* 115: 14–40.

Helffrich G, Stein S, and Wood BJ (1989) Subduction zone thermal structure and mineralogy and their relationship to seismic wave reflections and conversions at the slab/mantle interface. *Journal of Geophysical Research* 94: 753–763.

Helffrich GR and Wood BJ (1996) 410-km discontinuity sharpness and the form of the olivine α–β phase diagram: Resolution of apparent seismic contradictions. *Geophysical Journal International* 126: F7–F12.

Helffrich GR and Wood BJ (2001) The Earth's mantle. *Nature* 412: 501–507.

Hermance JF (1995) Electrical conductivity models of the crust and mantle. In: Ahrens TJ (ed.) *Global Earth Physics: A Handbook of Physical Constants, AGU Reference Shelf*, vol. 1, pp. 190–205. Washington, DC: American Geophysical Union.

Hernlund JW and Houser C (2008) On the statistical distribution of seismic velocities in Earth's deep mantle. *Earth and Planetary Science Letters* 265: 423–437.

Hernlund JW and Jellinek AM (2010) Dynamics and structure of a stirred partially molten ultralow-velocity zone. *Earth and Planetary Science Letters* 296: 1–8.

Hier-Majumder S and Courtier A (2011) Seismic signature of small melt fraction atop the transition zone. *Earth and Planetary Science Letters* 308: 334–342.

Hirose K, Fei Y, Ma Y, and Mao H-K (1999) The fate of subducted basaltic crust in the Earth's lower mantle. *Nature* 397: 53–56.

Hirose K and Lay T (2008) Discovery of post-perovskite and new views on the core–mantle boundary region. *Elements* 4: 183–189.

Hirose K, Takafuji N, Sata N, and Ohishi Y (2005) Phase transition and density of subducted MORB crust in the lower mantle. *Earth and Planetary Science Letters* 237: 239–251.

Hirschmann MM (2006) Water, melting, and the deep Earth H_2O cycle. *Annual Review of Earth and Planetary Sciences* 34: 629–653.

Hirschmann MM and Stolper EM (1996) A possible role for garnet pyroxenite in the origin of the "garnet signature" in MORB. *Contributions to Mineralogy and Petrology* 124: 185–208.

Hofmann AW and White WW (1982) Mantle plumes from ancient oceanic crust. *Earth and Planetary Science Letters* 57: 421–436.

Hosoya T, Kubo T, Ohtani E, Sano A, and Funakoshi K (2005) Water controls the fields of metastable olivine in cold subducting slabs. *Geophysical Research Letters* 32: L17305.

Houser C, Masters G, Flanagan M, and Shearer P (2008) Determination and analysis of long-wavelength transition zone structure using SS precursors. *Geophysical Journal International* 174: 178–194.

Humphreys ED, Dueker KG, Schutt DL, and Smith RB (2000) Beneath Yellowstone: Evaluating plume and nonplume models using teleseismic images of the upper mantle. *Geological Society of America - GSA Today* 10(12): 1–7.

Irifune T, Higo Y, Inoue T, Kono Y, Ohfuji H, and Funakoshi K (2008) Sound velocities of majorite garnet and the composition of the mantle transition region. *Nature* 451: 814–817.

Irifune T and Isshiki M (1998) Iron partitioning in a pyrolite mantle and the nature of the 410-km seismic discontinuity. *Nature* 392: 702–705.

Irifune T and Ringwood AE (1993) Phase transformations in subducted oceanic crust and buoyancy relationships at depths of 600–800 km in the mantle. *Earth and Planetary Science Letters* 117: 101–110.

Irifune T, Shinmei T, McCammon CA, Miyajima N, Rubie DC, and Frost DJ (2010) Iron partitioning and density changes of pyrolite in Earth's lower mantle. *Science* 327: 193–195.

Ishii M and Tromp J (1999) Normal-mode and free-air gravity constraints on lateral variations in velocity and density of the Earth's mantle. *Science* 285: 1231–1236.

Ishii M and Tromp J (2004) Constraining large-scale mantle heterogeneity using mantle and inner-core sensitive normal modes. *Physics of the Earth and Planetary Interiors* 146: 113–124.

Ita JJ and Stixrude L (1992) Petrology, elasticity and composition of the transition zone. *Journal of Geophysical Research* 97: 6849–6866.

Ivan M and Cormier VF (2011) High frequency PKKPBC around 2.5 Hz recorded globally. *Pure and Applied Geophysics* 168: 1759–1768.

Jackson I (1983) Some geophysical constraints on the chemical composition of the Earth's lower mantle. *Earth and Planetary Science Letters* 62: 91–103.

Jackson I (1998) Elasticity, composition and temperature of the Earth's lower mantle: A reappraisal. *Geophysical Journal International* 134: 291–311.

James DE, Boyd FR, Schutt D, Bell DR, and Carlson RW (2004) Xenolith constraints on seismic velocities in the upper mantle beneath southern Africa. *Geochemistry, Geophysics, Geosystems* 5: Q01002.

James DE, Fouch MJ, Carlson RW, and Roth JB (2011) Slab fragmentation, edge flow and the origin of the Yellowstone hotspot track. *Earth and Planetary Science Letters* 311: 124–135.

Jasbinsek J and Dueker K (2007) Ubiquitous low-velocity layer atop the 410-km discontinuity in the northern Rocky Mountains. *Geochemistry, Geophysics, Geosystems* 8: Q10004.

Jeanloz J (1995) Earth dons a different mantle. *Nature* 378: 130–131.

Jeanloz J and Knittle E (1989) Density and composition of the lower mantle. *Philosophical Transactions of the Royal Society Series A* 328: 377–389.

Jiang F, Gwanmesia GD, Dyuzheva TI, and Duffy TS (2009) Elasticity of stishovite and acoustic mode softening under high pressure by Brillouin scattering. *Physics of the Earth and Planetary Interiors* 172: 235–240.

Jiang G, Zhao D, and Zhang G (2008) Seismic evidence for a metastable olivine wedge in the subducting Pacific slab under Japan Sea. *Earth and Planetary Science Letters* 270: 300–307.

Kaneshima S and Helffrich G (1998) Detection of lower mantle scatterers northeast of the Mariana subduction zone using short-period array data. *Journal of Geophysical Research* 103: 4825–4838.

Kaneshima S and Helffrich G (1999) Dipping low-velocity layer in the mid-lower mantle: Evidence for geochemical heterogeneity. *Science* 283: 1888–1892.

Kaneshima S and Helffrich G (2009) Lower mantle scattering profiles and fabric below Pacific subduction zones. *Earth and Planetary Science Letters* 282: 234–239.

Kaneshima S and Helffrich G (2010) Small scale heterogeneity in the mid-lower mantle beneath the circum-Pacific area. *Physics of the Earth and Planetary Interiors* 183: 91–103.

Kaneshima S, Okamoto T, and Takenaka H (2007) Evidence for a metastable olivine wedge inside the subducted Mariana slab. *Earth and Planetary Science Letters* 258: 219–227.

Karato S-i (1997) On the separation of crustal component from subducted oceanic lithosphere near the 660 km discontinuity. *Physics of the Earth and Planetary Interiors* 99: 103–111.

Karki BB, Stixrude L, and Crain J (1997) Ab initio elasticity of three high-pressure polymorphs of silica. *Geophysical Research Letters* 24: 3269–3272.

Katsura T and Ito E (1989) The system Mg_2SiO_4-Fe_2SiO_4 at high pressures and temperatures: Precise determination of stabilities of olivine, modified spinel, and spinel. *Journal of Geophysical Research* 94: 15663–15670.

Katsura T, Yoneda A, Yamazaki D, Yoshino T, and Ito E (2010) Adiabatic temperature profile in the mantle. *Physics of the Earth and Planetary Interiors* 183: 212–218.

Kaus BJP, Connolly JAD, Podladchikov YY, and Schmalholz SM (2005) Effect of mineral phase transitions on sedimentary basin subsidence and uplift. *Earth and Planetary Science Letters* 233: 213–228.

Kawakatsu H and Watada S (2007) Seismic evidence for deep-water transportation in the mantle. *Science* 316: 1468–1471.

Kawakatsu H and Yoshioka S (2011) Metastable olivine wedge and deep dry cold slab beneath southwest Japan. *Earth and Planetary Science Letters* 303: 1–10.

Keller WR, Anderson DL, and Clayton RW (2000) Resolution of tomographic models of the mantle beneath Iceland. *Geophysical Research Letters* 27: 3993–3996.

Kennett BLN, Engdahl ER, and Buland R (1995) Constraints on seismic velocities in the Earth from traveltimes. *Geophysical Journal International* 122: 108–124.

Kerr RA (2003) Plumes from the core lost and found. *Science* 299: 35–36.

Kesson SE, Fitzgerald JD, and Shelley JMG (1998) Mineralogy and dynamics of a pyrolite lower mantle. *Nature* 393: 252–255.

Khan A, Kuvshinov A, and Semenov A (2011) On the heterogeneous electrical conductivity structure of the Earth's mantle with implications for transition zone water content. *Journal of Geophysical Research* 116: B01103.

Kirby S, Stein S, Okal E, and Rubie D (1996) Metastable mantle phase transformations and deep earthquakes in subducting oceanic lithosphere. *Reviews of Geophysics* 34: 261–306.

Koppers AAP (2011) Mantle plumes persevere. *Nature Geoscience* 4: 816–817.

Kubo T, Ohtani E, and Funakoshi K (2004) Nucleation and growth kinetics of the α–β transformation in Mg_2SiO_4 determined by in situ synchrotron powder X-ray diffraction. *American Mineralogist* 89: 285–293.

Kumazawa M, Sawamoto H, Ohtani E, and Masaki K (1974) Post-spinel phase of forsterite and evolution of the Earth's mantle. *Nature* 247: 356–358.

Lawrence JF and Shearer PM (2006) A global study of transition zone thickness using receiver functions. *Journal of Geophysical Research* 111: B06307.

Lawrence JF and Shearer PM (2008) Imaging mantle transition zone thickness with SdS-SS finite-frequency sensitivity kernels. *Geophysical Journal International* 174: 143–158.

Lay T and Garnero EJ (2011) Deep mantle seismic modeling and imaging. *Annual Review of Earth and Planetary Sciences* 39: 91–123.

Lay T, Hernlund J, Garnero EJ, and Thorne MS (2006) A post-perovskite lens and D" heat flux beneath the central Pacific. *Science* 24: 1272–1276.

Lay T, Williams Q, and Garnero EJ (1998) The core-mantle boundary layer and deep Earth dynamics. *Nature* 392: 461–468.

Lebedev S, Chevrot S, and van der Hilst RD (2002) Seismic evidence for olivine phase changes at the 410- and 660-kilometer discontinuities. *Science* 296: 1300–1302.

Li B (2003) Compressional and shear wave velocities of ringwoodite γ-Mg_2SiO_4 to 12 GPa. *American Mineralogist* 88: 1312–1317.

Li X, Kind R, Priestley K, et al. (2000) Mapping the Hawaiian plume conduit with converted seismic waves. *Nature* 405: 938–941.

Li X, Kind R, Yuan X, et al. (2003) Seismic observation of narrow plumes in the oceanic upper mantle. *Geophysical Research Letters* 30: 1334.

Li B and Liebermann RC (2007) Indoor seismology by probing the Earth's interior by using sound velocity measurements at high pressures and temperatures. *Proceedings of the National Academy of Sciences of the United States of America* 104: 9145–9150.

Li B, Liebermann RC, and Weidner DJ (2001) P-V-V_P-V_S-T measurements on wadsleyite to 7 GPa and 873 K: Implications for the 410-km seismic discontinuity. *Journal of Geophysical Research* 106: 30575–30591.

Li B, Rigden SM, and Liebermann RC (1996) Elasticity of stishovite at high pressure. *Physics of the Earth and Planetary Interiors* 96: 113–127.

Li J, Struzhkin VV, Mao HK, et al. (2004) Electronic spin state of iron in lower mantle perovskite. *Proceedings of the National Academy of Sciences of the United States of America* 101: 14027–14030.

Lin JF, Mao Z, Jarrige I, et al. (2010) Resonant X-ray emission study of the lower-mantle ferropericlase at high pressures. *American Mineralogist* 95: 1125–1131.

Lin JF and Tsuchiya T (2008) Spin transition of iron in the Earth's lower mantle. *Physics of the Earth and Planetary Interiors* 170: 248–259.

Lin JF, Vankó G, Jacobsen SD, et al. (2007) Spin transition zone in Earth's lower mantle. *Science* 317: 1740–1743.

Litasov K and Ohtani E (2007) Effect of water on the phase relations in Earth's mantle and deep water cycle. In: Ohtani E (ed.) *Advances in High-Pressure Mineralogy, GSA Special Papers* 421, pp. 115–156. Boulder, CO: Geological Society of America.

Litasov KD, Ohtani E, and Sano A (2006) Influence of water on major phase transitions in the Earth's mantle. In: Jacobsen S and van der Lee S (eds.) *Earth's Deep Water Cycle, Geophysical Monograph Series*, vol. 168, pp. 95–111. Washington, DC: American Geophysical Union.

Litasov KD, Ohtani E, Suzuki A, Kawazoe T, and Funakoshi K (2004) Absence of density crossover between basalt and peridotite in the cold slabs passing through 660 km discontinuity. *Geophysical Research Letters* 31: L24607.

Liu Z-K and Ågren J (1995) Thermodynamics of constrained and unconstrained equilibrium systems and their phase rules. *Journal of Phase Equilibria* 16: 30–35.

Liu J, Topor L, Zhang J, Navrotsky A, and Liebermann RC (1996) Calorimetric study of the coesite-stishovite transformation and calculation of the phase boundary. *Physics and Chemistry of Minerals* 23: 11–16.

Mao Z, Jacobsen SD, Jiang F, Smyth JR, Holl CM, and Duffy TS (2008) Elasticity of hydrous wadsleyite to 12 GPa: Implications for Earth's transition zone. *Geophysical Research Letters* 35: L21305.

Mao Z, Lin JF, Scott HP, et al. (2011) Iron-rich perovskite in the Earth's lower mantle. *Earth and Planetary Science Letters* 309: 179–184.

Mao HK, Shen G, and Hemley RJ (1997) Multivariable dependence of Fe/Mg partitioning in the Earth's lower mantle. *Science* 278: 2098–2100.

Marquardt H, Speziale S, Reichmann HJ, Frost DJ, Schilling FR, and Garnero EJ (2009) Elastic shear anisotropy of ferropericlase in Earth's lower mantle. *Science* 324: 224–226.

Masters G and Gubbins D (2003) On the resolution of density in the Earth. *Physics of the Earth and Planetary Interiors* 140: 159–167.

Matsukage KN, Jing Z, and Karato S (2005) Density of hydrous silicate melt at the conditions of Earth's deep upper mantle. *Nature* 438: 488–491.

Matsuno T, Seama N, Evans RL, et al. (2010) Upper mantle electrical resistivity structure beneath the central Mariana subduction system. *Geochemistry, Geophysics, Geosystems* 11: Q09003.

Mattern E, Matas J, Ricard Y, and Bass J (2005) Lower mantle composition and temperature from mineral physics and thermodynamic modeling. *Geophysical Journal International* 160: 973–990.

Matyska C and Yuen DA (2007) Lower-mantle material properties and convection models of multiscale plumes. In: Foulger GR and Jurdy DM (eds.) *Plates, Plumes and Planetary Processes, GSA Special Papers* 430, pp. 137–163. Boulder, CO: Geological Society of America.

Matyska C, Yuen DA, Wentzcovitch RM, and Čížková H (2011) The impact of variability in the rheological activation parameters on lower-mantle viscosity stratification and its dynamics. *Physics of the Earth and Planetary Interiors* 188: 1–8.

McCammon CA (1997) Perovskite as a possible sink for ferric iron in the lower mantle. *Nature* 387: 694–696.

McDonough WF and Rudnick RL (1998) Mineralogy and composition of the upper mantle. *Reviews in Mineralogy* 37: 139–164.

Melbourne T and Helmberger D (1998) Fine structure of the 410-km discontinuity. *Journal of Geophysical Research* 103: 10091–10102.

Montagner J-P and Ritsema J (2001) Interactions between ridges and plumes. *Science* 294: 1472–1473.

Mosenfelder JL, Marton FC, Ross CR, Kerschhofer L, and Rubie DC (2001) Experimental constraints on the depth of olivine metastability in subducting lithosphere. *Physics of the Earth and Planetary Interiors* 127: 165–180.

Murakami M, Hirose K, Kawamura K, Sata N, and Ohishi Y (2004) Post-perovskite phase transition in $MgSiO_3$. *Science* 304: 855–858.

Nakagawa T, Tackley PJ, Deschamps F, and Connolly JAD (2010) The influence of MORB and harzburgite composition on thermo-chemical mantle convection in a 3-D spherical shell with self-consistently calculated mineral physics. *Earth and Planetary Science Letters* 296: 403–412.

Neele F, de Regt H, and VanDecar J (1997) Gross errors in upper-mantle discontinuity topography from underside reflection data. *Geophysical Journal International* 129: 194–204.

Niu F and Kawakatsu H (1997) Depth variation of the mid-mantle seismic discontinuity. *Geophysical Research Letters* 24: 429–432.

Niu F, Kawakatsu H, and Fukao Y (2003) Seismic evidence for a chemical heterogeneity in the midmantle: A slightly dipping and strong seismic reflector at mid-mantle depth beneath the Mariana subduction zone. *Journal of Geophysical Research* 108(B9): 2419.

Niu F, Solomon SC, Silver PG, Suetsugu D, and Inoue H (2002) Mantle transition-zone structure beneath the South Pacific Superswell and evidence for a mantle plume underlying the Society hotspot. *Earth and Planetary Science Letters* 198: 371–380.

Oganov AR, Martoňák R, Laio A, Raiteri P, and Parrinello M (2005) Anisotropy of Earth's D" layer and stacking faults in the $MgSiO_3$ post-perovskite phase. *Nature* 438: 1142–1144.

Oganov AR and Ono S (2004) Theoretical and experimental evidence for a post-perovskite phase of $MgSiO_3$ in Earth's D" layer. *Nature* 430: 445–448.

Ohta K, Cohen RE, Hirose K, Haule K, Shimizu K, and Ohishi Y (2012) Experimental and theoretical evidence for pressure-induced metallization in FeO with the rock-salt type structure. *Physical Review Letters* 108: 026403.

Ohta K, Hirose K, Lay T, Sata N, and Ohishi Y (2008) Phase transitions in pyrolite and MORB at lowermost mantle conditions: Implications for a MORB-rich pile above the core-mantle boundary. *Earth and Planetary Science Letters* 267: 107–117.

Ohtani E (2005) Water in the mantle. *Elements* 1: 25–30.

Ohtani E and Litasov KD (2006) The effect of water on mantle phase transitions. *Reviews in Mineralogy and Geochemistry* 62: 397–420.

Ono S and Yasuda A (1996) Compositional change of majoritic garnet in a MORB composition from 7 to 17 GPa and 1400 to 1600°C. *Physics of the Earth and Planetary Interiors* 96: 171–179.

Peacock SM (1993) The importance of blueschist → eclogite dehydration reactions in subducting oceanic crust. *Geological Society of America Bulletin* 105: 684–694.

Pognante U (1989) Tectonic implications of lawsonite formation in the Sesia zone (western Alps). *Tectonophysics* 162: 219–227.

Reinsch D (1979) Glaucophanites and eclogites from Val Chiusella, Sesia-Lanzo zone (Italian Alps). *Contributions to Mineralogy and Petrology* 70: 257–266.

Resovsky J and Trampert J (2003) Using probabilistic seismic tomography to test mantle velocity-density relationships. *Earth and Planetary Science Letters* 215: 121–134.

Ricard Y, Mattern E, and Matas J (2005) Synthetic tomographic images of slabs from mineral physics. In: van der Hilst RD, Bass JD, Matas J, and Trampert J (eds.) *Earth's Deep Mantle: Structure, Composition, and Evolution, Geophysical Monograph Series*, vol. 160, pp. 283–300. Washington, DC: American Geophysical Union.

Ricolleau A, Perrillat J-P, Fiquet G, et al. (2010) Phase relations and equation of state of a natural MORB: Implications for the density profile of subducted oceanic crust in the Earth's lower mantle. *Journal of Geophysical Research* 115: B08202.

Ringwood AE (1975) *Composition and Petrology of the Earth's Mantle*. New York: McGraw-Hill.

Ringwood AE (1989) Constitution and evolution of the mantle. In: *Kimberlites and Related Rocks: Proceedings of the Fourth International Kimberlite Conference, Perth 1986, Geological Society of Australia Special Publication* 14, pp. 457–485. Sydney: Geological Society of Australia.

Ringwood AE and Irifune T (1988) Nature of the 650-km seismic discontinuity: Implications for mantle dynamics and differentiation. *Nature* 331: 131–136.

Ritsema J, van Heijst HJ, and Woodhouse JH (1999) Complex shear wave velocity structure imaged beneath Africa and Iceland. *Science* 286: 1925–1928.

Rost S, Garnero EJ, and Williams Q (2008) Seismic array detection of subducted oceanic crust in the lower mantle. *Journal of Geophysical Research* 113: B06303.

Sakamaki T, Suzuki A, and Ohtani E (2006) Stability of hydrous melt at the base of the Earth's upper mantle. *Nature* 439: 192–194.

Saltzer RL and Humphreys ED (1997) Upper mantle P wave velocity structure of the eastern Snake River Plain and its relationship to geodynamic models of the region. *Journal of Geophysical Research* 102: 11829–11841.

Schaeffer AJ and Bostock M (2010) A low-velocity zone atop the transition zone in northwestern Canada. *Journal of Geophysical Research* 115: B06302.

Shearer PM and Flanagan MP (1999) Seismic velocity and density jumps across the 410- and 660-kilometer discontinuities. *Science* 285: 1545–1548.

Shen Y, Solomon SC, Bjarnason IT, and Wolfe CJ (1998) Seismic evidence for a lower mantle origin of the Iceland plume. *Nature* 395: 62–65.

Shieh SR, Duffy TS, and Li B (2002) Strength and elasticity of SiO_2 across the stishovite-$CaCl_2$-type structural phase boundary. *Physical Review Letters* 89(25): 255507.

Simmons NA, Forte AM, Boschi L, and Grand SP (2010) GyPSuM: A joint tomographic model of mantle density and seismic wave speeds. *Journal of Geophysical Research* 115: B12310.

Simmons NA and Gurrola H (2000) Multiple seismic discontinuities near the base of the transition zone in the Earth's mantle. *Nature* 405: 559–562.

Sinmyo R, Hirose K, Muto S, Ohishi Y, and Yasuhara A (2011) The valence state and partitioning of iron in the Earth's lowermost mantle. *Journal of Geophysical Research* 116: B07205.

Sinogeikin SV, Katsura T, and Bass JD (1998) Sound velocities and elastic properties of Fe-bearing wadsleyite and ringwoodite. *Journal of Geophysical Research* 103: 20819–20825.

Smyth JR and Frost DJ (2002) The effect of water on the 410-km discontinuity: An experimental study. *Geophysical Research Letters* 29(10): 1485.

Solomatov VS and Stevenson DJ (1994) Can sharp seismic discontinuities be caused by non-equilibrium phase transformations? *Earth and Planetary Science Letters* 125: 267–279.

Song T-RA, Helmberger DV, and Grand SP (2004) Low-velocity zone atop the 410-km seismic discontinuity in the northwestern United States. *Nature* 427: 530–533.

Stixrude L (1997) Structure and sharpness of phase transitions and mantle discontinuities. *Journal of Geophysical Research* 102: 14835–14852.

Stixrude L, de Koker N, Sun N, Mookherjee M, and Karki BB (2009) Thermodynamics of silicate liquids in the deep Earth. *Earth and Planetary Science Letters* 278: 226–232.

Stixrude L, Hemley RJ, Fei Y, and Mao HK (1992) Thermoelasticity of silicate perovskite and magnesiowüstite and stratification of the Earth's mantle. *Science* 257: 1099–1101.

Stixrude L and Lithgow-Bertelloni C (2010) Thermodynamics of the Earth's mantle. *Reviews in Mineralogy and Geochemistry* 71: 465–484.

Stixrude L and Lithgow-Bertelloni C (2012) Geophysics of chemical heterogeneity in the mantle. *Annual Review of Earth and Planetary Sciences* 40: 569–595.

Su W and Dziewonski AM (1991) Predominance of long-wavelength heterogeneity in the mantle. *Nature* 352: 121–126.

Takenaka S, Sanshadokoro H, and Yoshioka S (1999) Velocity anomalies and spatial distributions of physical properties in horizontally lying slabs beneath the Northwestern Pacific region. *Physics of the Earth and Planetary Interiors* 112: 137–157.

Tarits P, Hautot S, and Perrier F (2004) Water in the mantle: Results from electrical conductivity beneath the French Alps. *Geophysical Research Letters* 31: L06612.

Tauzin B, Debayle E, and Wittlinger G (2010) Seismic evidence for a global low-velocity layer within the Earth's upper mantle. *Nature Geoscience* 3: 718–721.

Thomas C, Kendall J-M, and Helffrich G (2009) Probing two low velocity regions with PKP B-caustic amplitudes and scattering. *Geophysical Journal International* 178: 503–512.

Thompson DA, Helffrich G, Bastow ID, et al. (2011) Implications of a simple mantle transition zone beneath cratonic North America. *Earth and Planetary Science Letters* 312: 28–36.

Thorne MS and Garnero EJ (2004) Inferences on ultralow-velocity zone structure from a global analysis of SPdKS waves. *Journal of Geophysical Research* 109: B08301.

Tsuchiya T, Caracas R, and Tsuchiya J (2004a) First principles determination of the phase boundaries of high-pressure polymorphs of silica. *Geophysical Research Letters* 31(11): L11610.

Tsuchiya T, Tsuchiya J, Umemoto K, and Wentzcovitch RM (2004b) Elasticity of post-perovskite $MgSiO_3$. *Geophysical Research Letters* 31: L14603.

Tsuchiya T and Tsuchiya J (2008) Postperovskite phase equilibria in the $MgSiO_3$-Al_2O_3 system. *Proceedings of the National Academy of Sciences of the United States of America* 105: 19160–19164.

Vacher P, Mocquet A, and Sotin C (1998) Computation of seismic profiles from mineral physics: The importance of the non-olivine components for explaining the 660 km depth discontinuity. *Physics of the Earth and Planetary Interiors* 106: 275–298.

Vacher P, Spakman W, and Wortel MJR (1999) Numerical tests on the seismic visibility of metastable minerals in subduction zones. *Earth and Planetary Science Letters* 170: 335–349.

van der Lee S, Paulssen H, and Nolet G (1994) Variability of P660s phases as a consequence of topography on the 660 km discontinuity. *Physics of the Earth and Planetary Interiors* 86: 147–164.

van der Meijde M, Marone F, Giardini D, and van der Lee S (2003) Seismological evidence for water deep in Earth's upper mantle. *Science* 300: 1556–1558.

Van Keken PE, Karato S, and Yuen DA (1996) Rheological control of oceanic crust separation in the transition zone. *Geophysical Research Letters* 23: 1821–1824.

VanDecar JC, James DE, and Assumpção M (1995) Seismic evidence for a fossil mantle plume beneath South America and implications for plate driving forces. *Nature* 378: 25–31.

Velímský J (2010a) Electrical conductivity in the lower mantle: Constraints from CHAMP satellite data by time-domain EM induction modeling. *Physics of the Earth and Planetary Interiors* 180: 111–117.

Velímský J (2010b) Can we detect the conductivity decrease due to the iron spin transition in the mid-mantle? *20th IAGA WG 1.2 Workshop on Electromagnetic Induction in the Earth* Giza, Egypt, September 18–24, 2010. Abstract S9–9.

Vinnik L, Chevrot S, and Montagner J-P (1997) Evidence for a stagnant plume in the transition zone? *Geophysical Research Letters* 24: 1007–1010.

Walck MC (1984) The P-wave upper mantle structure beneath an active spreading center: The Gulf of California. *Geophysical Journal of the Royal Astronomical Society* 76: 697–723.

Walker D and Agee C (1989) Partitioning "equilibrium", temperature gradients, and constraints on Earth differentiation. *Earth and Planetary Science Letters* 96: 49–60.

Walter MJ, Kohn SC, Araujo D, et al. (2011) Deep mantle cycling of oceanic crust: Evidence from diamonds and their mineral inclusions. *Science* 334: 54–57.

Wang Y, Weidner DJ, and Guyot F (1996) Thermal equation of state of $CaSiO_3$ perovskite. *Journal of Geophysical Research* 101: 661–672.

Weidner DJ (1986) Mantle model based on measured physical properties of minerals. In: Saxena SK (ed.) *Chemistry and Physics of Terrestrial Planets*, pp. 251–274. New York: Springer-Verlag.

Wicks JK, Jackson JM, and Sturhahn W (2010) Very low sound velocities in iron-rich (Mg, Fe)O: Implications for the core-mantle boundary region. *Geophysical Research Letters* 37: L15304.

Wolfe CJ, Bjarnason IT, VanDecar JC, and Solomon SC (1997) Seismic structure of the Iceland mantle plume. *Nature* 385: 245–247.

Wood BJ (1987) Thermodynamics of multicomponent systems containing several solid solutions. *Reviews in Mineralogy* 17: 71–95.

Wood BJ (1995) The effect of H_2O on the 410-kilometer seismic discontinuity. *Science* 268: 74–76.

Wood BJ, Pawley A, and Frost DR (1996) Water and carbon in the Earth's mantle. *Philosophical Transactions of the Royal Society Series A* 354: 1495–1511.

Wood BJ and Rubie DC (1996) The effect of alumina on phase transformations at the 660 kilometer discontinuity from Fe-Mg partitioning experiments. *Science* 273: 1522–1524.

Wood BJ and Yuen DA (1983) The role of lithospheric phase transitions on seafloor flattening at old ages. *Earth and Planetary Science Letters* 66: 303–314.

Woodward RL and Masters G (1991) Lower mantle structure from ScS-S differential travel times. *Nature* 352: 231–233.

Wookey J, Stackhouse S, Kendall J-M, Brodholt J, and Price GD (2005) Efficacy of the post-perovskite phase as an explanation for lowermost-mantle seismic properties. *Nature* 438: 1004–1007.

Xu W, Lithgow-Bertelloni C, Stixrude L, and Ritsema J (2008) The effect of bulk composition and temperature on mantle seismic structure. *Earth and Planetary Science Letters* 275: 70–79.

Zaug JM, Abramson EH, Brown JM, and Slutsky LJ (1993) Sound velocities in olivine at Earth mantle pressures. *Science* 260: 1487–1489.

Zha CS, Duffy TS, Downs RT, Mao H-K, and Hemley RJ (1998a) Brillouin scattering and X-ray diffraction of San Carlos olivine: Direct pressure determination to 32 GPa. *Earth and Planetary Science Letters* 159: 25–33.

Zha CS, Duffy TS, Downs RT, Mao H-K, Hemley RJ, and Weidner DJ (1998b) Single crystal elasticity of the α and β of Mg_2SiO_4 polymorphs at high pressure. In: Manghnani MH and Yagi T (eds.) *Properties of Earth and Planetary Materials at High Pressure and Temperature, Geophysical Monograph Series*, vol. 101, pp. 9–16. Washington, DC: American Geophysical Union.

Zhang F and Oganov AR (2006) Valence state and spin transition of iron in Earth's mantle silicates. *Earth and Planetary Science Letters* 249: 436–443.

Zhang Y, Ritsema J, and Thorne M (2009) Modeling the ratios of SKKS and SKS amplitudes with ultra-low velocity zones at the core–mantle boundary. *Geophysical Research Letters* 36: L19303.

Zhang R-Q, Wu Q-J, Li Y-H, and Zeng RS (2011) Differential patterns of SH and P wave velocity structures in the transition zone beneath northwestern Tibet. *Science China Earth Sciences* 54: 1551–1562.

Zhao Y and Anderson DL (1994) Mineral physics constraints on the chemical composition of the Earth's lower mantle. *Physics of the Earth and Planetary Interiors* 85: 273–292.